Investigation of Nickel Oxide / Perovskite Interfacial in Inverted Perovskite Solar Cell

CHEE CHEW YEE

UNIVERSITI TEKNIKAL MALAYSIA MELAKA

INVESTIGATION OF NICKEL OXIDE / PEROVSKITE INTERFACIAL IN INVERTED PEROVSKITE SOLAR CELL

CHEE CHEW YEE

This report is submitted in partial fulfilment of the requirements for the degree of Bachelor of Electronic Engineering with Honours

Faculty of Electronic and Computer Engineering
Universiti Teknikal Malaysia Melaka

2023

DECLARATION

I declare that this report entitled "Investigation of Nickel Oxide / Perovskite Interfacial in Inverted Perovskite Solar Cell" is the result of my own work except for quotes as cited in the references.

Signature : ……………………………………

Author : CHEE CHEW YEE

Date : 13/1/2023

APPROVAL

I hereby declare that I have read this thesis and in my opinion this thesis is sufficient in terms of scope and quality for the award of Bachelor of Electronic Engineering with Honours.

Signature : ....

Supervisor Name : ....

DR. ZUL ATFYI FAUZAN BIN MOHAMMED NAPIAH
Senior Lecturer
Faculty of Electronics and Computer Engineering
Universiti Teknikal Malaysia Melaka (UTeM)
Hang Tuah Jaya, 76100
Durian Tunggal, Melaka, Malaysia

Date : 13/01/2023

DEDICATION

I dedicate this thesis to my beloved parents, Mr. Chee Kong Wing and Mrs. Ng Guat Wan, my supervisor, Dr. Zul Atfyi Fauzan bin Mohammed Napiah, and co-supervisor, Dr. Muhammad Idzdihar bin Idris, as well as all my friends, seniors, and colleagues for their moral support, cooperation, encouragement, and understanding throughout my educational pursuit. Thank you very much.

ABSTRACT

Inverted perovskite solar cells (IPSC) have gotten a lot of interest in recent years because of their consistent operational stability, reduced hysteresis, and low fabrication procedure. Among the materials used in p-type semiconductor, NiOx is the most widely applied as the hole transport layer (HTL) because the organic HTL has poor stability and complicated doping process. However, NiOx has some drawbacks, which are low conductivity and unsatisfactory interface contact with perovskite. In this project, the work is divided into two sections. The first section was simulation of IPSC, and the second section was the deposition and characterization of NiOx/MAPbI3 layer. For the first section, the focus of this project was on simulating NiOx as HTL in IPSC using the GPVDM software. The simulated results were evaluated by extracting the important parameters such as power conversion efficiency (PCE), short circuit current density (Jsc), open circuit voltage (Voc) and fill factor on different variation of layers. A complete modelling device structure of ITO/NiOx/MAPbI3/C60/BCP/Ag was successfully simulated with better PCE, which is 18.227% compared to previous work, which is 17.57%. For the second section, the project was focused to characterize the NiOx/MAPbI3, which is synthesized by sol-gel method. Then, the deposited layers were characterized by UV-Vis, SEM and XRD.

It was found that the annealed NiOx/MAPbI3 has improved the performance and stability, resulting in a good stability compared with non-anneal NiOx/MAPbI3. From these findings, the ITO/NiOx/MAPbI3/C60/BCP/Ag in IPSC has a potential for the development of IPSC with higher PCE.

ABSTRAK

Sel suria perovskit tersongsang (IPSC) telah mendapat perhatian sejak beberapa tahun ini kerana kestabilan operasi yang konsisten, histeresis yang berkurangan dan prosedur pembikinan yang rendah. Antara bahan yang digunakan dalam semikonduktor jenis-p, NiOx adalah yang paling banyak digunakan sebagai lapisan pengangkutan lubang (HTL) kerana HTL organik mempunyai kestabilan yang lemah dan proses doping yang rumit. Walau bagaimanapun, NiOx mempunyai beberapa kelemahan, iaitu kekonduksian rendah dan hubungan antara muka yang tidak memuaskan dengan perovskit. Projek ini dibahagikan kepada dua bahagian. Bahagian pertama adalah simulasi IPSC, dan bahagian kedua ialah pemendapan dan pencirian lapisan NiOx/MAPbI3. Untuk bahagian pertama, tumpuan projek ini adalah untuk mensimulasikan NiOx sebagai HTL dalam IPSC menggunakan perisian GPVDM. Hasil simulasi dinilai dengan mengekstrak parameter penting seperti kecekapan penukaran kuasa (PCE), ketumpatan arus litar pintas (Jsc), voltan litar terbuka (Voc) dan faktor isian pada variasi lapisan yang berbeza. Model struktur ITO/NiOx/MAPbI3/C60/BCP/Ag yang lengkap telah berjaya disimulasikan dengan PCE yang lebih baik, iaitu 18.227% berbanding kerja sebelumnya, iaitu 17.57%. Untuk bahagian kedua, projek ini difokuskan untuk mencirikan

NiOx/MAPbI3, yang disintesis dengan kaedah sol-gel. Kemudian, lapisan yang dimendapkan dicirikan oleh UV-Vis, SEM dan XRD. Didapati bahawa penyepuhlindapan NiOx/MAPbI3 telah meningkatkan prestasi dan kestabilan yang menghasilkan jangka hayat yang lebih lama berbanding dengan NiOx/MAPbI3 tanpa penyepuhlindapan. Daripada penemuan penyiasatan ini, ITO/NiOx/MAPbI3/C60/BCP/Ag dalam IPSC mempunyai potensi untuk pembangunan IPSC dengan PCE yang lebih tinggi.

ACKNOWLEDGEMENTS

This Bachelor Degree Project and the report was successfully completed with given timeline. First and foremost, student wishes to express her gratitude to her supervisor, Dr. Zul Atfyi Fauzan bin Mohammed Napiah, and co-supervisor, Dr. Muhammad Idzdihar bin Idris, for patiently guiding her throughout these two semesters and helping her in reviewing reports, presentation slides, and project output.

Aside from that, student is grateful to her beloved senior, Subathra Muniandy and friends who have always been willing to provide a hand when needed. Student would like to thank her parents for their unwavering support and encouragement during difficult times, which inspired her to keep striving.

Lastly, student gladly thank to faculty for providing well equipped lab that greatly aided in the completion of this project. Student believes that this project will be helpful for present and future use. Also, hoping the use of technology in the society, this project will be beneficial.

TABLE OF CONTENTS

Declaration

Approval

Dedication

LIST OF FIGURES

LIST OF TABLES

LIST OF SYMBOLS AND ABBREVIATIONS

HTL : Hole transport layer

NiOx : Nickel Oxide

IPSC : Inverted Perovskite Solar Cell

α : Absorption coefficient

n : Refractive index

Voc : Open circuit voltage

Jsc : Circuit current density

FF : Fill factor

PCE : Power Conversion Efficiency

PV : Photovoltaic

ITO : Indium Tin Oxide

FTO : Fluorine doped Tin Oxide

ETL : Electron transport layer

HTL : Hole transport layer

PEDOT: PSS : Poly (3,4-ethylenedioxythiophene) polystyrene sulfonate

PCBM : Phenyl C-61 Butyric acid methyl ester

Rs : High serial resistance

PSCs : Perovskite solar cells

C_{60} : Fullerene

BCP : Bathocuproine

IPA : Isopropyl alcohol

KOH : Potassium Hydroxide

$C_4H_6NiO_4$: Nickel (II) Acetate

MAI : Methylammonium iodide

PbI_2 : Lead (II) iodide

DMSO : Dimethyl sulfoxide

DMF : Dimethylformamide

CHAPTER 1

INTRODUCTION

The project introduction is covered in this chapter. Furthermore, it emphasizes the issue of the current state of industry, which leads to the project's development. In addition, the research background, objective, problem statement and scope of work will all be covered in this chapter.

1.1 Project background

With the fast expansion of society and the economy, excessive use of fossil fuels has created significant concerns such as energy shortages, environmental harm, and global warming. Therefore, renewable energy is frequently at the top of any discussion on how the globe might mitigate the worst effects of increasing temperatures. The researchers are motivated to maximize the generation of renewable energy in order to solve climate change challenges.

According to Shahzad (2015), renewable energy is the energy which is derived from a limitless source [1]. Renewable energy is also often referred to as clean energy due to the fact that renewable energy sources like sun and wind do not create carbon dioxide or other greenhouse gases, which contribute to global warming. Figure 1.1 show the example of generic renewable energy technologies.

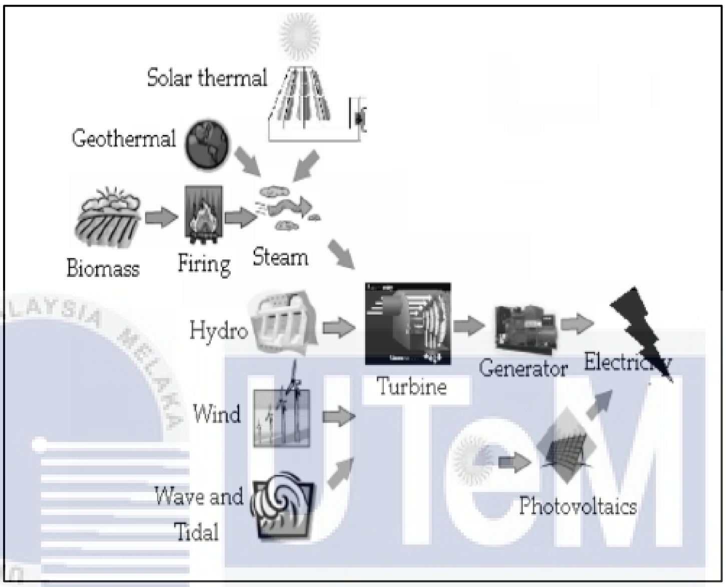

Figure 1.1: Generic renewable energy. [2]

For the planet Earth, the sun is a primary source of unlimited free energy such as solar energy. This energy may be harvested directly for use in homes, companies, schools, and hospitals using a variety of technologies. Photovoltaic cells and panels, are one of the examples of solar energy technology. PV is a type of active solar technology that was discovered in 1839 by Alexandre-Edmond Becquerel, a 19-year-old French physicist. Photovoltaic cells are semiconductor devices that convert light energy to electrical energy. There are three generations of solar PV technologies as shown in Figure 1.2.

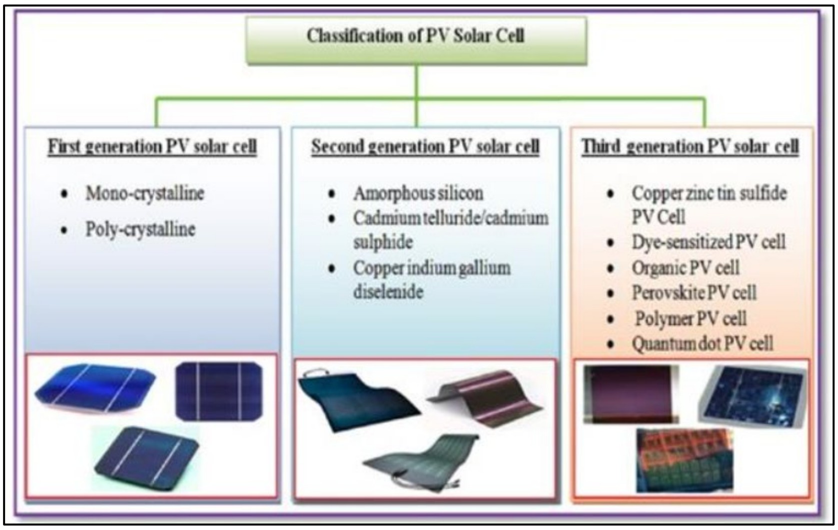

Figure 1.2: The generation of solar PV cells

The underlying technology for first-generation PV cells is silicon wafer technology. This generation includes monocrystalline and polycrystalline silicon PV cells. The solar cell of this generation is more efficient and lasts longer than other PV cells. However, the cost of production is higher, and it easily degrade at higher temperatures [1].

Thin film PV technology is used to produce second generation PV cells. In comparison to the first generation of PV cells, they are simpler and use fewer semiconductor materials. The third generation PV cells, on the other hand, are designed to manufacture high-efficiency devices using thin-film technology, as opposed to the second-generation PV cells.

Therefore, in this project focus on Inverted Perovskite Solar (IPSC), which is under the third generation of solar PV cells. IPSC is a form of solar cell that uses a perovskite-structured compound as the light-harvesting active layer, most typically a hybrid organic-inorganic lead or tin halide-based material. In inverted p-i-n perovskite solar cells, the HTL is deposited first and the light falls first on HTL before it encounters ETL. Figure 1.3 showed the general structure of IPSC. Inverted p-i-n (substrate/HTL/perovskite/ETL/top electrode) have attracted a lot of attention due to their simple device fabrication technique, high power conversion efficiency (PCE), and low hysteresis.

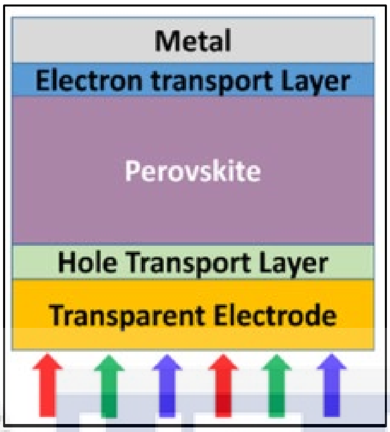

Figure 1.3: General structure of IPSC. [2]

ITO or FTO glass is commonly used as the transparent electrode. These glasses are transparent conductive substrate. The electron transport layer (ETL) is responsible for extracting electrons from the perovskite layer and preventing recombination between electrons in the ITO or FTO and holes in the perovskite layer. Perovskite is used to transport the electric charge whenever the light presents in the material. Hole transport layer (HTL) is used to covers the perovskite and collects the hole. HTL can be organic or inorganic. Lastly, metal is used as back contact.

1.2 Problem statement

Spiro-OMeTAD and PEDOT: PSS are frequently employed as HTL, but the complicated doping process and poor stability of organic HTL make them not so promising for real applications [3]. Alternatively, inorganic p-type semiconductors, specially NiOx which is the most widely used as HTL can provide intrinsically higher stability and exhibits lower cost compared to organic polymer-based HTL.

However, NiOx has some drawbacks such as intrinsic low conductivity of NiOx [4] and unsatisfactory interface contact between NiOx and perovskite. [5].The low conductivity of NiOx results in increased charge carrier recombination and degraded hole extraction efficiency. Moreover, the interface contact issue of the NiOx film with a perovskite layer not only influences the interfacial charge transfer but also affects perovskite crystallite growth.

Thus, in this project will simulate NiOx as HTL, then deposit the NiOx / $MAPbI_3$, which synthesized by sol-gel method to investigate the interface contact in NiOx on perovskite.

1.3 Project objective

The project aims to simulate nickel oxide as HTL in the inverted perovskite solar cell using GPVDM. Secondly, to evaluate the performance of simulated IPSC by extracting the important parameters such as PCE, fill factor, open-circuit voltage and short circuit photocurrent on different variation of layers in GPVDM software. Lastly, to characterize the NiOx / $MAPbI_3$ layer, which is synthesized by sol-gel method.

1.4 Project scope

This project scope involves the simulation of IPSC by using GPVDM software. NiOx is chosen as inorganic material as HTL. Then, the important parameters are extracted from the simulation, such as PCE is used to evaluate the efficiency of IPSC on different variation such as electrical parameters, thickness of active layers in the simulation, temperature dependency, absorption coefficient (α) and refractive index

(n) of the material used in GPVDM. The important parameters are compared with the reference result for PCE, Voc, Jsc and FF are 17.57%, 1.042V, 21.72mA cm^{-2} and 0.776 which previously done by the researchers [4]. Once the outcome is desired, the NiOx / MAPbI$_3$ layer will be deposited by using sol-gel method. Characterizations of the NiOx / MAPbI$_3$ layer will be measured by using X-Ray Diffractometer, UV Visible spectrophotometer and Scanning Electron Microscope (SEM).

1.5 Environment and sustainability

Due to abundant raw materials and low processing costs, with a quick energy payback and low overall CO$_2$ emissions, this project is environmentally friendly and sustainable. Unlike typical fossil fuel technologies, solar cell does not actively emit any emissions when convert solar energy to electrical energy. As a non - polluting source of energy, perovskite solar cells are good to the environment. Thus, this project fulfills the Sustainable Development Goal 7, which aim to access to an affordable, reliable and sustainable energy.

Figure 1.4: Sustainable Development Goal – Clean energy

CHAPTER 2

BACKGROUND STUDY

A literature review surveys books, scholarly articles, and any other sources relevant to a particular issue, area of research, or theory. Moreover, it is based on a past project that is comparable to this project. This part focuses on the investigation and examination of methods and equipment utilized by other researchers. As a result, this part determined the methodologies, strengths, and limitations of this project in order to improve the solar cell's efficiency.

2.1 Inverted perovskite solar cell

Perovskite materials as an alternative for silicon as the absorber layer of solar cells grabbed researchers' attention as silicon-based solar cell technology neared its limit. The PCE of IPSC has grown dramatically in recent years, from 3.8 % for the first prototype to approved 23.72% which is an exceptional efficiency when compared to other thin film photovoltaics [32]. In order to investigate the interfacial contact between NiOx and perovskite, researches about the both layers of IPSC structure have been done.

2.2 Hole transport layer

Hole transport layers play an important role in the performance characteristics of n-i-p and p-i-n perovskite solar cell. Also, stability and power conversion efficiencies are heavily dependent on the transporting layers used in the IPSC structure [6]. Therefore, the light to power conversion efficiency in PSCs can be drastically improved by optimizing the hole transport layer with appropriate materials. Short circuits are usually avoided by using a thick layer of HTL. Nevertheless, thick HTL layers can also cause high serial resistance (Rs). The hole transport layers can be divided into three categories, which are organic HTL, Polymeric HTL and Inorganic HTL. Only the first and third category will be discussed in this sub chapter.

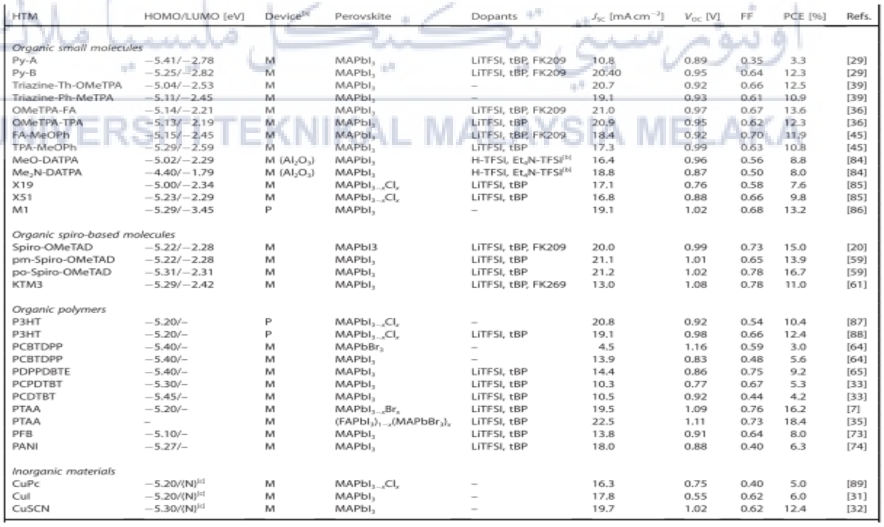

HTM	HOMO/LUMO [eV]	Device[a]	Perovskite	Dopants	J_{sc} [mA cm^{-2}]	V_{oc} [V]	FF	PCE [%]	Refs.
Organic small molecules									
Py-A	−5.41/−2.78	M	MAPbI$_3$	LiTFSI, tBP, FK209	10.8	0.89	0.35	3.3	[29]
Py-B	−5.25/−2.82	M	MAPbI$_3$	LiTFSI, tBP, FK209	20.40	0.95	0.64	12.3	[29]
Triazine-Th-OMeTPA	−5.04/−2.53	M	MAPbI$_3$	–	20.7	0.92	0.66	12.5	[39]
Triazine-Ph-MeTPA	−5.11/−2.45	M	MAPbI$_3$	–	19.1	0.93	0.61	10.9	[39]
OMeTPA-FA	−5.14/−2.21	M	MAPbI$_3$	LiTFSI, tBP, FK209	21.0	0.97	0.67	13.6	[36]
OMeTPA-TPA	−5.13/−2.19	M	MAPbI$_3$	LiTFSI, tBP	20.9	0.95	0.62	12.3	[36]
FA-MeOPh	−5.15/−2.45	M	MAPbI$_3$	LiTFSI, tBP, FK209	18.4	0.92	0.70	11.9	[45]
TPA-MeOPh	−5.29/−2.59	M	MAPbI$_3$	LiTFSI, tBP	17.3	0.99	0.63	10.8	[45]
MeO-DATPA	−5.02/−2.29	M (Al$_2$O$_3$)	MAPbI$_3$	H-TFSI, Et$_4$N-TFSI[b]	16.4	0.96	0.56	8.8	[84]
Me$_2$N-DATPA	−4.40/−1.79	M (Al$_2$O$_3$)	MAPbI$_3$	H-TFSI, Et$_4$N-TFSI[b]	18.8	0.87	0.50	8.0	[84]
X19	−5.00/−2.34	M	MAPbI$_{3-x}$Cl$_x$	LiTFSI, tBP	17.1	0.76	0.58	7.6	[85]
X51	−5.23/−2.29	M	MAPbI$_{3-x}$Cl$_x$	LiTFSI, tBP	16.8	0.88	0.66	9.8	[85]
M1	−5.29/−3.45	P	MAPbI$_3$	–	19.1	1.02	0.68	13.2	[86]
Organic spiro-based molecules									
Spiro-OMeTAD	−5.22/−2.28	M	MAPbI3	LiTFSI, tBP, FK209	20.0	0.99	0.73	15.0	[20]
pm-Spiro-OMeTAD	−5.22/−2.28	M	MAPbI$_3$	LiTFSI, tBP	21.1	1.01	0.65	13.9	[59]
po-Spiro-OMeTAD	−5.31/−2.31	M	MAPbI$_3$	LiTFSI, tBP	21.2	1.02	0.78	16.7	[59]
KTM3	−5.29/−2.42	M	MAPbI$_3$	LiTFSI, tBP, FK269	13.0	1.08	0.78	11.0	[61]
Organic polymers									
P3HT	−5.20/–	P	MAPbI$_{3-x}$Cl$_x$	–	20.8	0.92	0.54	10.4	[87]
P3HT	−5.20/–	P	MAPbI$_{3-x}$Cl$_x$	LiTFSI, tBP	19.1	0.98	0.66	12.4	[88]
PCBTDPP	−5.40/–	M	MAPbBr$_3$	–	4.5	1.16	0.59	3.0	[64]
PCBTDPP	−5.40/–	M	MAPbI$_3$	–	13.9	0.83	0.48	5.6	[64]
PDPPDBTE	−5.40/–	M	MAPbI$_3$	LiTFSI, tBP	14.4	0.86	0.75	9.2	[65]
PCPDTBT	−5.30/–	M	MAPbI$_3$	LiTFSI, tBP	10.3	0.77	0.67	5.3	[33]
PCDTBT	−5.45/–	M	MAPbI$_3$	LiTFSI, tBP	10.5	0.92	0.44	4.2	[33]
PTAA	−5.20/–	M	MAPbI$_{3-x}$Br$_x$	LiTFSI, tBP	19.5	1.09	0.76	16.2	[7]
PTAA	–	M	(FAPbI$_3$)$_{1-x}$(MAPbBr$_3$)$_x$	LiTFSI, tBP	22.5	1.11	0.73	18.4	[35]
PFB	−5.10/–	M	MAPbI$_3$	LiTFSI, tBP	13.8	0.91	0.64	8.0	[73]
PANI	−5.27/–	M	MAPbI$_3$	LiTFSI, tBP	18.0	0.88	0.40	6.3	[74]
Inorganic materials									
CuPc	−5.20/(N)[d]	M	MAPbI$_{3-x}$Cl$_x$	–	16.3	0.75	0.40	5.0	[89]
CuI	−5.20/(N)[d]	M	MAPbI$_3$	–	17.8	0.55	0.62	6.0	[31]
CuSCN	−5.30/(N)[d]	M	MAPbI$_3$	–	19.7	1.02	0.62	12.4	[32]

Figure 2.1: Summary of highest performing HTL. [7]

The standard organic perovskite cells normally use PEDOT: PSS and Spiro-OMeTAD as the HTL. Figure above is the summary of highest performing HTL.

According to Ameen et al. (2016), who reported that due of poor hole transport through the device, pristine Spiro-OMeTAD is effectively a poorly conducting insulator, making devices to tend to have Rs [7] . Besides, Ghosh et al. (2019) reported that although these organic materials provide high efficiency, but unable to improve the stability [8]. This view is also supported by Arumugam et al. (2021), which stated that due to their acidic and hygroscopic character, as well as the expensive expense of preparation, large-scale productions were limited. As a result, various researchers are working on replacing organic HTL with other low-cost efficient HTMs that produce PSC devices with high efficiency and stability for commercial purposes.

Several experiments reported in the Pitchaiya et al. (2020) journal pointed out that the high cost of these organic materials, dopants, and additives [9]. These limitations have compelled researchers to seek out low-cost, long-lasting materials. This has allowed inorganic p-type materials including copper, nickel, and HTMs based on transition metal oxides such as CuI, NiOx, Cu_2O, CuO, MoOx, VOx, WOx to be used in the perovskite solar cells. This is because these inorganic transport layers encapsulate the absorber layer better, resulting in increased stability.

2.2.1 Inorganic HTL

Inorganic HTL materials have been used in solar cells, LEDs, and FETs, among other applications that have been investigated for decades. There are numerous vacancies currently available to focus on materials properties of perovskite solar cell, such as band matching of HTLs and compatibility of perovskite materials. The energy level graphs for commonly used inorganic hole transport materials in perovskite solar cells can be seen in Figure 2.2. They must have great mobility, conductivity, and mobility.

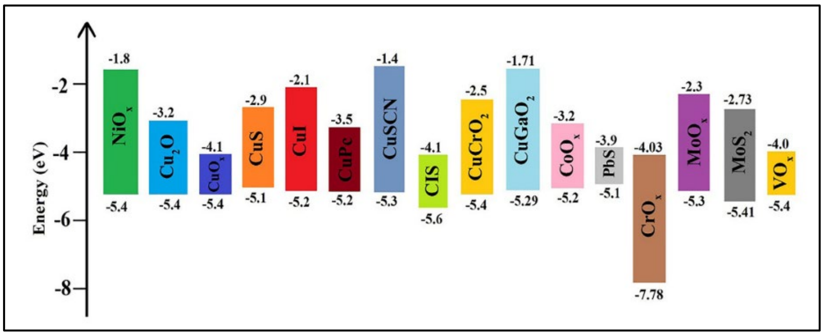

Figure 2.2: The energy level diagram for generally used inorganic HTL. [10]

2.2.2 NiOx

Nickel oxide (NiOx) is a promising HTL with its intrinsic p-type semiconductor characteristics, high transparency, wide bandgap and suitable work function with valence band (5.4 eV) which matched with the valence band of MAPbI$_3$ [10] [11]. However, the poor conductivity of NiOx causes more charge carrier recombination and worse hole extraction efficiency.

Many studies have shown that doping metal elements into NiOx can significantly increase electrical conductivity. According to the Park (2022), he mentioned that NiOx can be doped with a variety of elements such as Cu, Li, Mg, Cs, and Co to enhance conductivity and PSC efficiency by lowering interfacial resistance at the HTL/perovskite interface [12]. Figure 2.3 shows the parameters for NiOx and doped NiOx. This is supported by Ma et al. (2020). The doped NiOx films have increased conductivity and film quality, which is advantageous for interface charge extraction. Furthermore, as a consequence of the alloyed metal oxide properties of doped NiOx, enhanced work function of NiOx was absorbed, resulting in a more suitable energy level mitch with perovskite layer, which lower the voltage deficit. [13]

The statement is proved from other researches. Qiu et al. (2017) produced Li-doped NiOx films with greatly increased electrical conductivity, raising the PCE from 12.59% to 15.51%.[14] Moreover, Ag is another p-type doping for NiOx. Li et al. used a simple sol-gel approach to increase the PCE of IPSC from 13.46% to 16.86% for the 2 mol% Ag:NiOx-based device. They doped Ag by incorporating AgNO3 into the nickel nitrate solution at a rate of 1%, 2%, and 4%, respectively.[15] Furthermore, while deposited on Ag:NiOx, the crystallinity of perovskite was enhanced.

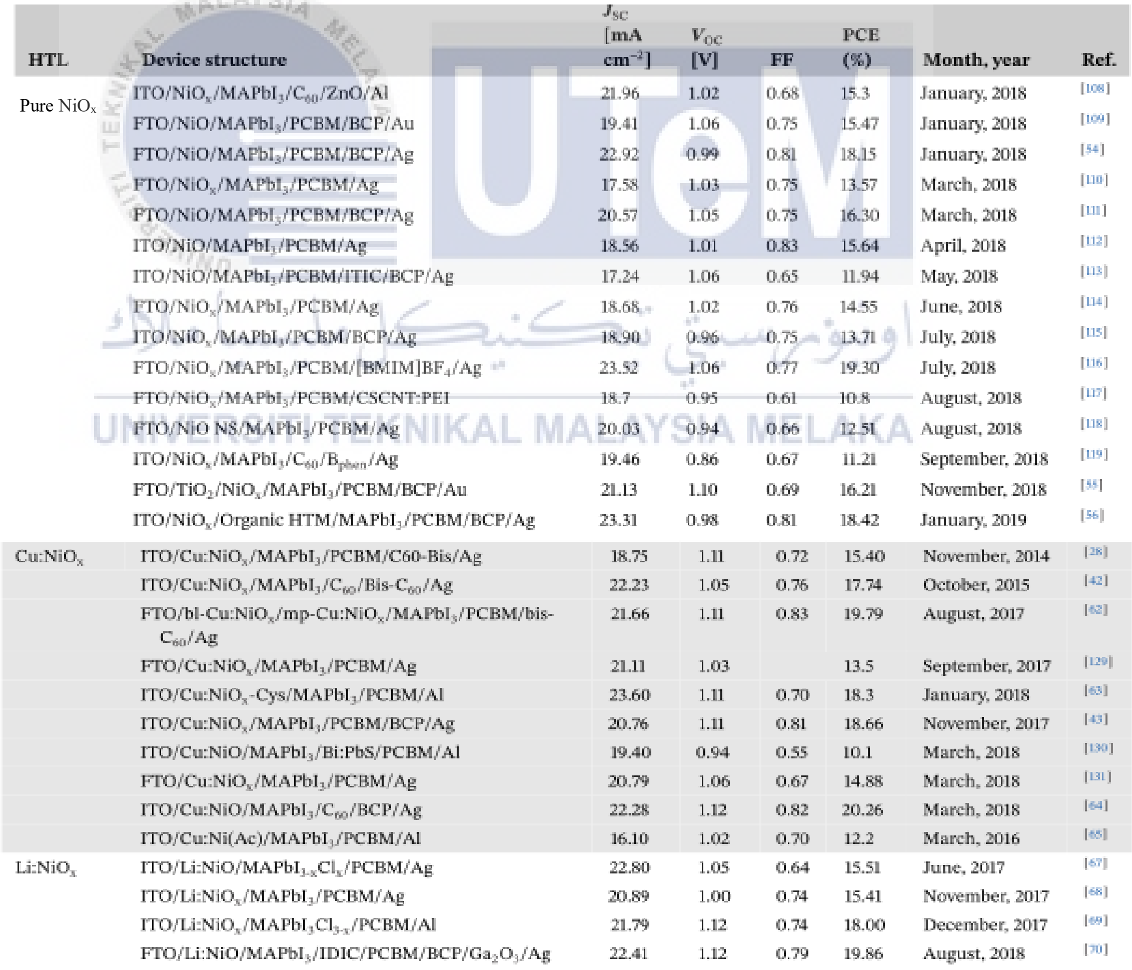

HTL	**Device structure**	**J_{SC} [mA cm^{-2}]**	**V_{OC} [V]**	**FF**	**PCE (%)**	**Month, year**	**Ref.**
Pure NiO_x	$ITO/NiO_x/MAPbI_3/C_{60}/ZnO/Al$	21.96	1.02	0.68	15.3	January, 2018	[108]
	$FTO/NiO/MAPbI_3/PCBM/BCP/Au$	19.41	1.06	0.75	15.47	January, 2018	[109]
	$FTO/NiO/MAPbI_3/PCBM/BCP/Ag$	22.92	0.99	0.81	18.15	January, 2018	[54]
	$FTO/NiO_x/MAPbI_3/PCBM/Ag$	17.58	1.03	0.75	13.57	March, 2018	[110]
	$FTO/NiO/MAPbI_3/PCBM/BCP/Ag$	20.57	1.05	0.75	16.30	March, 2018	[111]
	$ITO/NiO/MAPbI_3/PCBM/Ag$	18.56	1.01	0.83	15.64	April, 2018	[112]
	$ITO/NiO/MAPbI_3/PCBM/ITIC/BCP/Ag$	17.24	1.06	0.65	11.94	May, 2018	[113]
	$FTO/NiO_x/MAPbI_3/PCBM/Ag$	18.68	1.02	0.76	14.55	June, 2018	[114]
	$ITO/NiO_x/MAPbI_3/PCBM/BCP/Ag$	18.90	0.96	0.75	13.71	July, 2018	[115]
	$FTO/NiO_x/MAPbI_3/PCBM/[BMIM]BF_4/Ag$	23.52	1.06	0.77	19.30	July, 2018	[116]
	$FTO/NiO_x/MAPbI_3/PCBM/CSCNT:PEI$	18.7	0.95	0.61	10.8	August, 2018	[117]
	FTO/NiO NS$/MAPbI_3/PCBM/Ag$	20.03	0.94	0.66	12.51	August, 2018	[118]
	$ITO/NiO_x/MAPbI_3/C_{60}/B_{phen}/Ag$	19.46	0.86	0.67	11.21	September, 2018	[119]
	$FTO/TiO_2/NiO_x/MAPbI_3/PCBM/BCP/Au$	21.13	1.10	0.69	16.21	November, 2018	[55]
	$ITO/NiO_x/$Organic HTM$/MAPbI_3/PCBM/BCP/Ag$	23.31	0.98	0.81	18.42	January, 2019	[56]
$Cu:NiO_x$	$ITO/Cu:NiO_x/MAPbI_3/PCBM/C60\text{-}Bis/Ag$	18.75	1.11	0.72	15.40	November, 2014	[28]
	$ITO/Cu:NiO_x/MAPbI_3/C_{60}/Bis\text{-}C_{60}/Ag$	22.23	1.05	0.76	17.74	October, 2015	[42]
	$FTO/bl\text{-}Cu:NiO_x/mp\text{-}Cu:NiO_x/MAPbI_3/PCBM/bis\text{-}C_{60}/Ag$	21.66	1.11	0.83	19.79	August, 2017	[62]
	$FTO/Cu:NiO_x/MAPbI_3/PCBM/Ag$	21.11	1.03		13.5	September, 2017	[129]
	$ITO/Cu:NiO_x\text{-}Cys/MAPbI_3/PCBM/Al$	23.60	1.11	0.70	18.3	January, 2018	[63]
	$ITO/Cu:NiO_x/MAPbI_3/PCBM/BCP/Ag$	20.76	1.11	0.81	18.66	November, 2017	[43]
	$ITO/Cu:NiO/MAPbI_3/Bi:PbS/PCBM/Al$	19.40	0.94	0.55	10.1	March, 2018	[130]
	$FTO/Cu:NiO_x/MAPbI_3/PCBM/Ag$	20.79	1.06	0.67	14.88	March, 2018	[131]
	$ITO/Cu:NiO/MAPbI_3/C_{60}/BCP/Ag$	22.28	1.12	0.82	20.26	March, 2018	[64]
	$ITO/Cu:Ni(Ac)/MAPbI_3/PCBM/Al$	16.10	1.02	0.70	12.2	March, 2016	[65]
$Li:NiO_x$	$ITO/Li:NiO/MAPbI_{3-x}Cl_x/PCBM/Ag$	22.80	1.05	0.64	15.51	June, 2017	[67]
	$ITO/Li:NiO_x/MAPbI_3/PCBM/Ag$	20.89	1.00	0.74	15.41	November, 2017	[68]
	$ITO/Li:NiO_x/MAPbI_3Cl_{3-x}/PCBM/Al$	21.79	1.12	0.74	18.00	December, 2017	[69]
	$FTO/Li:NiO/MAPbI_3/IDIC/PCBM/BCP/Ga_2O_3/Ag$	22.41	1.12	0.79	19.86	August, 2018	[70]

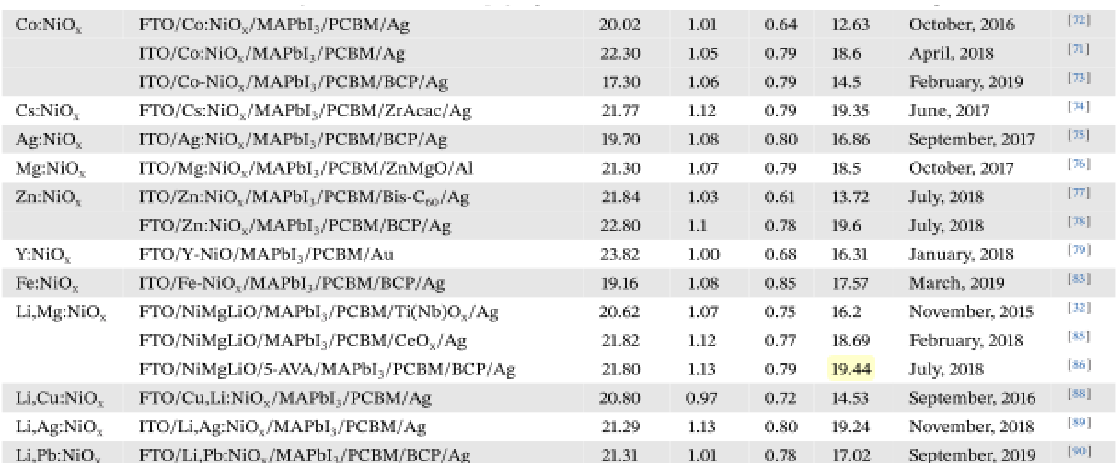

Co:NiO_x	FTO/Co:NiO_x/$MAPbI_3$/PCBM/Ag	20.02	1.01	0.64	12.63	October, 2016	[72]
	ITO/Co:NiO_x/$MAPbI_3$/PCBM/Ag	22.30	1.05	0.79	18.6	April, 2018	[71]
	ITO/Co-NiO_x/$MAPbI_3$/PCBM/BCP/Ag	17.30	1.06	0.79	14.5	February, 2019	[73]
Cs:NiO_x	FTO/Cs:NiO_x/$MAPbI_3$/PCBM/ZrAcac/Ag	21.77	1.12	0.79	19.35	June, 2017	[74]
Ag:NiO_x	ITO/Ag:NiO_x/$MAPbI_3$/PCBM/BCP/Ag	19.70	1.08	0.80	16.86	September, 2017	[75]
Mg:NiO_x	ITO/Mg:NiO_x/$MAPbI_3$/PCBM/ZnMgO/Al	21.30	1.07	0.79	18.5	October, 2017	[76]
Zn:NiO_x	ITO/Zn:NiO_x/$MAPbI_3$/PCBM/Bis-C_{60}/Ag	21.84	1.03	0.61	13.72	July, 2018	[77]
	FTO/Zn:NiO_x/$MAPbI_3$/PCBM/BCP/Ag	22.80	1.1	0.78	19.6	July, 2018	[78]
Y:NiO_x	FTO/Y-NiO/$MAPbI_3$/PCBM/Au	23.82	1.00	0.68	16.31	January, 2018	[79]
Fe:NiO_x	ITO/Fe-NiO_x/$MAPbI_3$/PCBM/BCP/Ag	19.16	1.08	0.85	17.57	March, 2019	[83]
Li,Mg:NiO_x	FTO/NiMgLiO/$MAPbI_3$/PCBM/Ti(Nb)O_x/Ag	20.62	1.07	0.75	16.2	November, 2015	[32]
	FTO/NiMgLiO/$MAPbI_3$/PCBM/CeO_x/Ag	21.82	1.12	0.77	18.69	February, 2018	[85]
	FTO/NiMgLiO/5-AVA/$MAPbI_3$/PCBM/BCP/Ag	21.80	1.13	0.79	19.44	July, 2018	[86]
Li,Cu:NiO_x	FTO/Cu,Li:NiO_x/$MAPbI_3$/PCBM/Ag	20.80	0.97	0.72	14.53	September, 2016	[88]
Li,Ag:NiO_x	ITO/Li,Ag:NiO_x/$MAPbI_3$/PCBM/Ag	21.29	1.13	0.80	19.24	November, 2018	[89]
Li,Pb:NiO_x	FTO/Li,Pb:NiO_x/$MAPbI_3$/PCBM/BCP/Ag	21.31	1.01	0.78	17.02	September, 2019	[90]

Figure 2.3 Pure and doped NiOx as inorganic HTLs based inverted organic-inorganic halide PVSCs: device architectures and photovoltaic characteristics. [10]

2.3 Interfacial between NiOx and $MAPbI_3$

According to Pitchaiya et al. (2020), with methylammonium lead iodide perovskite, NiOx works as a possible HTL and exhibits good hole transfer properties, resulting in increased device performance [9]. NiOx is non-corrosive to ITO substrates because to its inertness, and its work function makes it a good HTL for perovskite solar cell. However, Shen and his coworkers reported that NiOx has two drawbacks, which are intrinsic low conductivity and the poor interfacial contact between NiOx and perovskite. They also stated that the NiOx film's interface contact with a perovskite layer affects not just interfacial charge transfer but also perovskite crystallite development [4]. To tackle the problem, Shen and his coworkers propose a new facial method to enhance interface contact by changing the morphology and structure of the NiOx layers and producing high-performance PSCs based on bilayer-NiOx HTLs. The device had a PCE of 17.57% and was stable enough in ambient air.

Moreover, Chen et al. reported a hybrid interfacial layer of "compact NiO/mp-Al_2O_3" in an inverted PSCs device of CL-NiO/ Al_2O_3/$CH_3NH_3PbI_3$/PCBM/BCP/Ag with high PCE of 13.5% and outstanding V_{OC} of 1.04 V to decrease losses during light harvesting and charge transfer at interfaces. The "dual blocking impact" of this interfacial layer was significant. It serves as a barrier between the FTO and $CH_3NH_3PbI_3$, as well as helping to block shunt paths between NiOx and PCBM via the mp-Al_2O_3 layer loaded with perovskite crystals [14].

2.3.1 Comparison on deposition of NiOx and the enhancement for NiOx/Perovskite interface contact

Table 2.1 shows the comparison on the deposition of NiOx and the enhancement for NiOx/Perovskite interface contact between the previous researches.

Table 2.1: Comparison between research papers

No.	Title	Description	Ref.
1	Obstructing interfacial reaction between NiOx and perovskite to enable efficient and stable inverted perovskite solar cells	Device structure: ITO/NiOx/SaC-100/$MAPbI_3$/PCBM/BCP/Ag Synthesis method: Spin coating Main step: Trimethylolpropane tris(2-methyl-1-aziridinepropionate) (SaC-100) deposited onto NiOx Advantages: 1) Suppress the interaction between Ni^{3+} and MAI to increase conductivity and reduce interfacial defects, hence lowering Voc loss and improving device stability. 2) Perovskite morphology and interfacial energy level alignment are also optimized.	[16]

		Results: PCE, Voc, Jsc and FF are 20.21%, 1.12V, 22.37 mA cm^{-2} and 0.8126 respectively.	
2	Using Interfacial Contact Engineering to Solve Nickel Oxide/Perovskite Interface Contact Issues in Inverted Perovskite Solar Cells	Device structure: FTO/NiOx/$MAPbI_3$/C_{60}/BCP/Ag Synthesis method: Spin coating sol-gel Main step: Add PVB to NiOx precursor solution as chelating agent and bilayer NiOx film was designed. Advantages: 1) Enhance the NiOx/perovskite interface contact. 2) Bilayer NiOx can reduce the trap density and avoid the direct contact of FTO glass and perovskite. Results: PCE, Voc, Jsc and FF are 17.57%, 1.042V, 21.72 mA cm^{-2}, and 0.776 respectively.	[4]
3	Understanding the Doping Effect on NiO: Toward High-Performance Inverted Perovskite Solar Cells	Device structure: ITO/Cu:NiO/$CH_3NH_3PbI_3$/C_{60}/BCP/Ag Synthesis method: Spin coating Main step: NiOx is doped with Cu Advantages: Enhanced work function, along with increased conductivity, provides better charge transfer and extraction. Results: PCE, Voc, Jsc and FF are 20.26%, 1.12V, 22.28 mA cm^{-2} and 0.812 respectively.	[41]
4	NiO/Perovskite Heterojunction Contact Engineering for Highly Efficient and Stable Perovskite Solar Cells	Device structure: ITO/NiOx/CsBr/MA1−xFAxPbI3−yCly/phenyl-C61-butyric acid methylester/BCP/Ag Synthesis method: Spin coating Main step: CsBr was used as a buffer layer between the NiOx and perovskite layer to modulate the contact properties. Advantages: 1) Could relieve the interface stress 2) Enhance the quality of the perovskite film with large grain size.	[17]

		3) Increase charge extraction efficiency 4) Reduce the charge recombination Results: PCE, Voc, Jsc and FF are 19.7%, 1.10V, 23.7 mA cm^{-2} and 0.76 respectively.	
5	Oxidized Nickel films as highly transparent HTLs for inverted planar perovskite solar cells	Device structure: $FTO/NiO/MAPbI_3/PCBM/Au$ Synthesis method: Evaporation Main step: The Ni target was evaporated for varied durations of 70, 100, and 130 seconds at an optimal temperature of ~1200 °C. Advantages: Can form a highly transparent NiO thin films and complete coverage by perovskite absorbers overlayer resulted in the enhanced value of J_{SC}. Results: PCE, Voc, Jsc and FF are 9.71%, 0.97V, 20.66 mA cm^{-2} and 0.48 respectively.	[18]
6	Overcoming Redox Reactions at Perovskite-Nickel Oxide Interfaces to Boost Voltages in Perovskite Solar Cells	Device structure: $ITO/NiOx/Cs_{0.25}FA_{0.75}Pb(Br_{0.2}I_{0.8})_3/LiF/C_{60}/BCP/Ag$ Synthesis method: Spin coating sol- gel Main step: A-site post-treatments to the NiOx HTL or use of excess A-site such as FAI, FABr, CsI, and CsBr in the perovskite precursor solution. Advantages: In method 1: elimate reactive $Ni^{\geq 3+}$ sites before perovskite deposition In method 2: counteract the loss in organohalide that occurs in the reaction. Results: PCE, Voc, Jsc and FF are 19.06%, 1.15V, 19.56mA cm^{-2} and 0.847 respectively.	[5]
7	Highly Efficient and Uniform 1 cm^2 Perovskite Solar Cells with an Electrochemically Deposited NiOx Hole-Extraction Layer	Device structure: $ITO/NiO/MAPbI_3/PCBM/Ag$ Synthesis method: Electrodeposition Main step: As a counter electrode and a reference electrode, a platinum foil and an Ag/AgCl electrode were utilized, respectively. The deposition solution was nickel (II) nitrate	[19]

		hexahydrate, and the deposition current ranged from 0.05 to 0.5 mA cm^{-2}. Advantages : By altering the deposition current or voltage during the deposition process, the thickness and surface roughness of the NiOx layer can be accurately regulated in real time. Results: PCE, Voc, Jsc and FF are 17% (in $1.084cm^2$), 1.04 V, 22.5 mA cm^{-2} and 0.72 respectively.	
8	Engineered optical and electrical performance of rf–sputtered undoped nickel oxide thin films for inverted perovskite solar cells	Device structure: ITO/NiOx/$CH_3NH_3PbI_3$/PCBM/BCP/Ag Synthesis method: RF Sputtering Main step: RF magnetron sputtering was used to deposit the NiOx thin films from an 80mm-diameter NiOx target. The sputtering deposition power was 250W, and the deposition pressure was varied. Advantages: The deposition parameters are controllable in exact manner and conformal and compact flms are formed easily in the manner of mass production via this technique. Results: PCE, Voc, Jsc and FF are 10.1%, 0.964V, 14.83 mA cm^{-2} and 0.706 respectively.	[20]
9	High-Performance Inverted Perovskite Solar Cells with Mesoporous NiOx Hole Transport Layer by Electrochemical Deposition	Device structure: FTO/NiOx/$MAPbI_3$/PCBM/BCP/Ag Synthesis method: Electrodeposition Main step: The p-type NiOx layer was deposited on the cleaned FTO/glass substrate via applying constant current density of 0.1 mA cm^{-2} and subsequent annealing at 300 °C for 2 hours. Advantages: 1) Thickness of NiOx can be controlled by regulating the time and current. 2) Environmentally friendly and suitable for mass production.	[21]

		Results: PCE, Voc, Jsc and FF are 17.77% (with active area of 0.25cm^2), 1.014V, 21.55 mA cm^{-2} and 0.8134 respectively.	
10	Air-stable perovskite photovoltaic cells with low temperature deposited NiOx as an efficient hole-transporting material	Device structure: FTO/NiOx/$CH_3NH_3PbI_3$/PCBM/BCP/Ag Synthesis method: Electron beam physical vapor deposition (EBPVD, alongside sputtering) Main step: The deposition chamber pressure was approximately 4.6 x 104 Pa during deposition. The substrates were not heated (room temperature), and the deposition rate was lowered to 0.15 nm/s in order to achieve a film thickness of about 20 nm. Advantages: Well-dispersed, dense, high purity, and unwanted contamination-free NiOx film at low temperature with high material utilization. Results: PCE, Voc, Jsc and FF are 13.2%, 0.95V, 17.90 mA cm^{-2} and 0.77 respectively.	[22]
11	Room-Temperature-Sputtered Nanocrystalline Nickel Oxide as Hole Transport Layer for p–i–n Perovskite Solar Cells	Device structure: ITO/NiOx/$MAPbI_3$/PCBM/BCP/Ag Synthesis method: Sputtering Results: PCE, Voc, Jsc and FF are 17.60%, 1.078V, 20.65 mA cm^{-2}, 0.79respectively.	[23]
12	Structural and Electrical Investigation of Cobalt-Doped NiOx/Perovskite Interface for Efficient Inverted Solar Cells	Device structure: Glass/ITO/Co-NiOx/$CH_3NH_3PbI_3$ /PCBM/BCP/Ag Synthesis method: Cobalt-doped / Prepared by spin coating method Main step: Doping divalent cobalt (Co^{2+}), $CoCl_2 \cdot 6H_2O$ was added to the Ni $(NO_3)_2 \cdot 6H_2O$ solution at various molar ratios while the calcination temperature was set at 270 °C. Advantages: 1) Improve of the conductivity of NiOx 2) Increase of perovskite layer morphology	[24]

		Results: PCE, Voc, Jsc and FF are 16.42%, 1.005V, 21.5 mA cm^{-2} and 0.76 respectively.	
13	Solution-processed Sr-doped NiOx as hole transport layer for efficient and stable perovskite solar cells	Device structure: FTO/Sr:NiOx/Perovskite/PCBM/AgAl Synthesis method: Sr doped / Prepared by sol-gel method Main step: Sr-doped NiOx, SrCl2 dissolved in 2-methoxyethanol are mixed with the NiOx solution at different molar ratios. Advantages: Better conductivity and superior contact properties between FTO and perovskite layers, which aid in hole carrier transport and extraction. Results: PCE, Voc, Jsc and FF are 20.07%, 1.118V, 22.68 mA cm^{-2} and 0.79 respectively.	[25]
14	Performance Comparison between the Nanoporous NiOxLayer andNiOxThin Film for Inverted Perovskite Solar Cells with Long-TermStability	Device structure: FTO/Nanoporous NiOx/Perovskite/ PCBM/ TIPD/ Ag Synthesis method: Spin coating Main step: 8 mL of 0.1 M$NiSO_4\cdot 7H_2O$ was added to a solution of 6 mL of 0.025 M$K_2S_2O_8$ in DI water and 2 mL of aqueous ammonia (25−28 wt%). The mixed growth fluid was shaken and poured onto the Petri plate right away. After 5 minutes, the substrate was removed, washed with deionized water to remove any loose black particles, and dried at 100°C for 1 hour. Following drying, the substrate was placed in a high-temperature oven for 1 hour of calcination at 450°C. Advantages: Reduce charge recombination and improve JSC of devices Results: PCE, Voc, Jsc and FF are 13.43%, 1.02V, 18.9 mA cm^{-2} and 12.73 respectively.	[26]
15	Room temperature solution-processed Fe doped NiOx as a novel hole transport layer for high efficient perovskite solar cells	Device structure: ITO/ Fe:NiOx/ $CH_3NH_3PbI_3$/PCBM/BCP/Ag Synthesis method: Fe doped/ Prepared by spin coating Main step: Fe-doped NiOx (Fe-NiOx) NPs, different molar ratios of Fe $(NO_3)\cdot 9H_2O$ was	[27]

		added to the nickel nitrate solution, and the remaining procedures were similar to the synthesis of the pristine NiOx NPs. Advantages: Good electrical properties and improved hole extraction compared to pristine NiOx NPs. Results: PCE, Voc, Jsc and FF are 17.54%, 1.082V, 19.21 mA cm^{-2} and 0.85 respectively.	
16	Thermal Analysis of Metal-Organic Precursors for Functional Cu:NiOx Hole Transporting Layer in Inverted Perovskite Solar Cells: Role of Solution Combustion Chemistry in Cu:NiOx Thin Films Processing	Device structure: ITO/Cu:NiOx/perovskite/PCBM/BCP/Ag Synthesis method: Cu doped/ Combustion Main step: 0.95 mmol Ni $(NO_3)2.6H_2O$ and 0.05 mmol $Cu(NO_3)2.3H_2O$ were dissolved in 10 ml 2-methoxyethanol with different concentrations of fuel acetylacetonate to the solution and the mixture was further mixed for 1 h at room temperature. The samples were then dried for 5 minutes at 80 °C before being annealed for 1 hour. Advantages: Cost-effectiveness, simplicity, improve electronic material functioning, and need lower processing annealing temperatures Results: PCE, Voc, Jsc and FF are 16.58 %, 0.99 V, 21.40 mA cm^{-2} and 0.78 respectively.	[28]

2.4 Summary

To conclude all the sub topics in Chapter 2.1, although organic HTL is high in efficiency, but the stability is poor. Inorganic p-type semi-conductors as HTLs, on the other hand, have recently received greater attention because of their high stability, outstanding hole mobility, and reasonable hole collecting with easy, numerous, and low-cost production techniques.

Besides, the doped NiOx can significantly increase electrical conductivity to overcome the intrinsic low conductivity of NiOx and the poor interfacial contact between NiOx and perovskite. However, there is limitation for doping metal elements in NiOx. To dissolve these materials, there are toxic organic solvents often used, which is harmful to the environment.

To solve the problem, redesigning the morphology and structure of the NiO_x layers are applied. There are many ways to synthesis the NiOx layer, such as sputtering, electron beam physical vapor deposition, combustion, spin coating and evaporation. However, in this project, student will synthesis the NiOx layer by using sol gel method due to the method used is low cost, simplicity and reproductivity. Also, student will investigate and compare the anneal and non-anneal NiOx /$MaPbI_3$ to evaluate the stability and absorbance of the samples.

CHAPTER 3

METHODOLOGY

Methodology is closely linked to the rules and use of flow charts to show the journey of a project. The Gantt chart can also be used to show the activities performed during the duration of the project. All of the implementation steps, as well as the flow chart and Gantt chart, will be thoroughly detailed in this chapter.

3.1 Gantt Chart

The Gantt chart indicates when an event is expected to occur in the project by presenting an overview of the sequence in which the activites must be completed. Figure 3.1 shows the Gantt chart of the project.

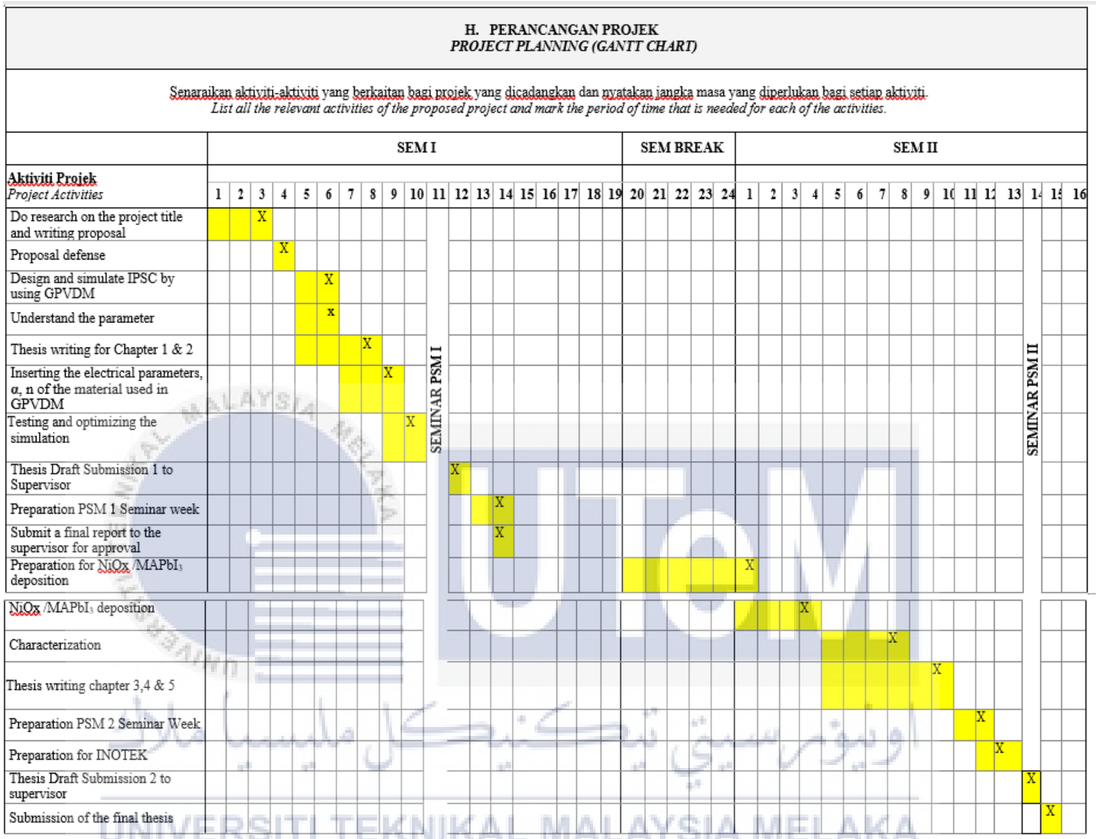

H. PERANCANGAN PROJEK
PROJECT PLANNING (GANTT CHART)

Senaraikan aktiviti-aktiviti yang berkaitan bagi projek yang dicadangkan dan nyatakan jangka masa yang diperlukan bagi setiap aktiviti.
List all the relevant activities of the proposed project and mark the period of time that is needed for each of the activities.

	SEM I																			SEM BREAK					SEM II															
Aktiviti Projek *Project Activities*	1	2	3	4	5	6	7	8	9	10	11	12	13	14	15	16	17	18	19	20	21	22	23	24	1	2	3	4	5	6	7	8	9	10	11	12	13	14	15	16
Do research on the project title and writing proposal	🟨	🟨	X								SEMINAR PSM I																											SEMINAR PSM II		
Proposal defense				X																																				
Design and simulate IPSC by using GPVDM					🟨	X																																		
Understand the parameter					🟨	x																																		
Thesis writing for Chapter 1 & 2					🟨	🟨	🟨	X																																
Inserting the electrical parameters, α, n of the material used in GPVDM							🟨	🟨	X																															
Testing and optimizing the simulation									🟨	X																														
Thesis Draft Submission 1 to Supervisor												X																												
Preparation PSM 1 Seminar week													🟨	X																										
Submit a final report to the supervisor for approval														X																										
Preparation for NiOx /MAPbI$_3$ deposition																				🟨	🟨	🟨	🟨	🟨	X															
NiOx /MAPbI$_3$ deposition																									🟨	🟨	🟨	X												
Characterization																													🟨	🟨	🟨	X								
Thesis writing chapter 3,4 & 5																													🟨	🟨	🟨	🟨	🟨	X						
Preparation PSM 2 Seminar Week																																			🟨	X				
Preparation for INOTEK																																				🟨	X			
Thesis Draft Submission 2 to supervisor																																						X		
Submission of the final thesis																																							X	

Figure 3.1: Gantt chart

3.2 Flow chart

The procedures that will be followed in this project is to search for and collect appropriate information depending on the project from various sources such as journals and books. Next, the layers in the IPSC will be designed and simulated using a software called GPVDM. This software is a free general-purpose simulation tool for optoelectronic devices. It was initially intended to simulate organic solar cells.

Nonetheless, it has been enhanced to simulate more device classes, such as OLEDs, OFETs, and a variety of other first, second, and third-generation solar cells. This software also aids in the study of the PCE, Voc, and FF obtained from the simulated IPSC.

Figure 3.2 is the flowchart for the part of simulation. Then, NiOx/MAPbI$_3$ layer will be deposited after the simulation. Figure 3.3 is the flowchart of the fabrication process.

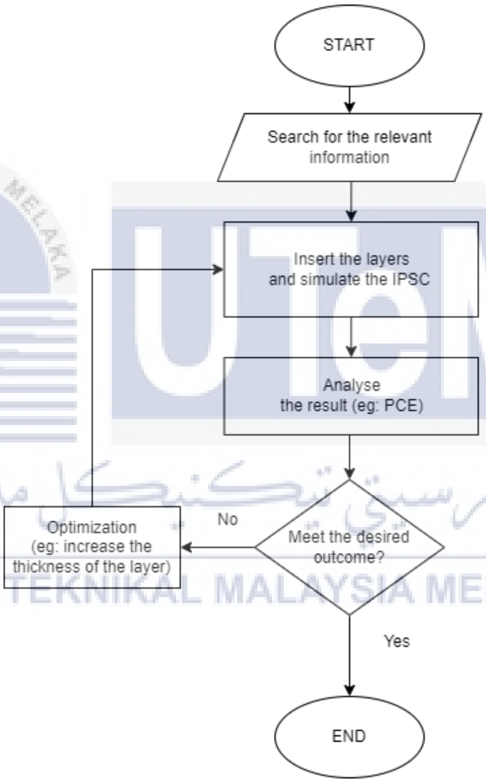

Figure 3.2: Flowchart of simulation process

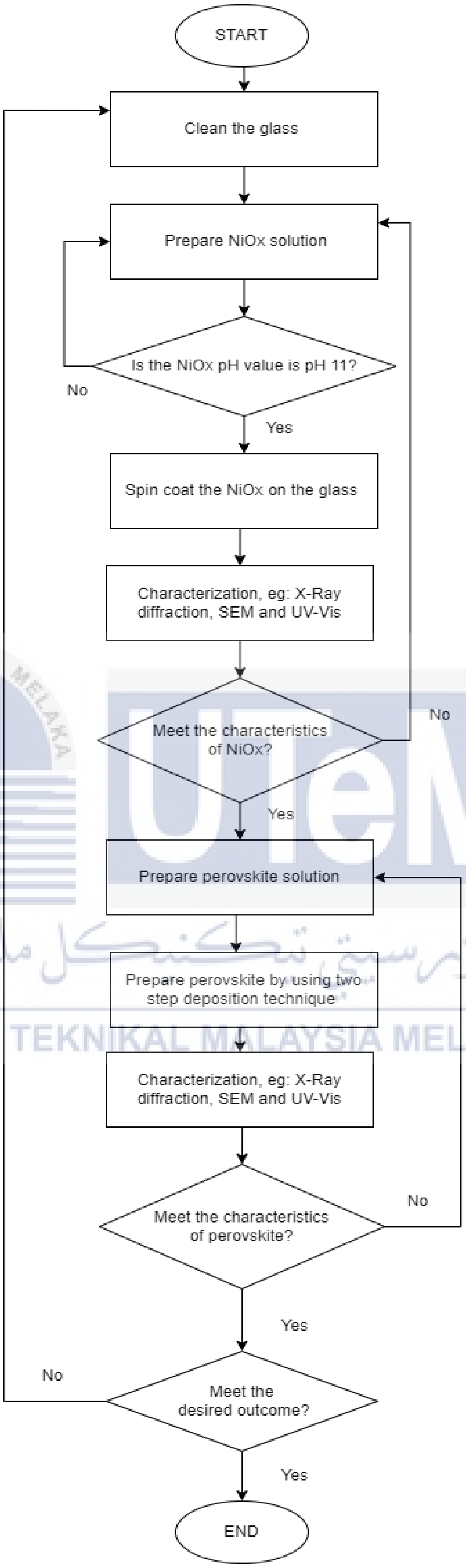

Figure 3.3: Flowchart of NiOx/$MAPbI_3$ deposition process

3.3 Research on electrical parameters in GPVDM for each active layer

The table below is the electrical parameter for the active layers in GPVDM, which are NiOx, $MAPbI_3$, BCP and C_{60}.

Table 3.1: The electrical parameters of the active layers

Parameters	NiOx [29][30]	$MAPbI_3$ [31][32]	BCP [33]	C_{60} [34]
Electron mobility ($m^2v^{-1}s^{-1}$)	0.0028	6.86×10^{-7}	1×10^{-7}	8×10^{-5}
Hole mobility ($m^2v^{-1}s^{-1}$)	0.0028	0.0375	2×10^{-7}	3.5×10^{-7}
Effective density of free electron states @300K (m^{-3})	1×10^{26}	5×10^{26}	2.2×10^{9}	8×10^{13}
Effective density of hole electron states (@300K) (m^{-3})	1×10^{26}	5×10^{26}	1.8×10^{12}	8×10^{13}
Electron affinity, Xi (eV)	1.46	1.6	3.9	3.9
Band gap, Eg (eV)	1.3	1.5	3.5	1.7
Relative permittivity	5	3	4	4.2

3.4 IPSC simulation

The process for simulating the IPSC using GPVDM, as indicated in subtopic 3.4.1 is outlined below. The technique for adding materials that are not in the GPVDM database is described in subtopic 3.4.2.

3.4.1 Procedure

1. Install the GPVDM software from https://www.gpvdm.com/.

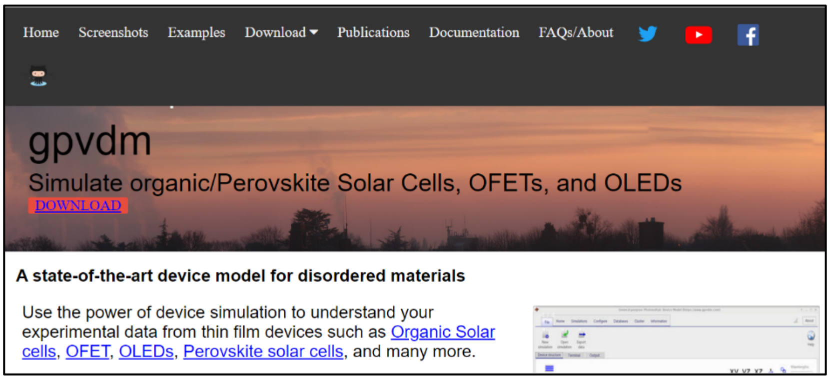

Simulate organic/Perovskite Solar Cells, OFETs, and OLEDs

A state-of-the-art device model for disordered materials

Use the power of device simulation to understand your experimental data from thin film devices such as Organic Solar cells, OFET, OLEDs, Perovskite solar cells, and many more.

Figure 3.4: GPVDM software

2. Click “New simulation”, then click inverted organic solar cell.

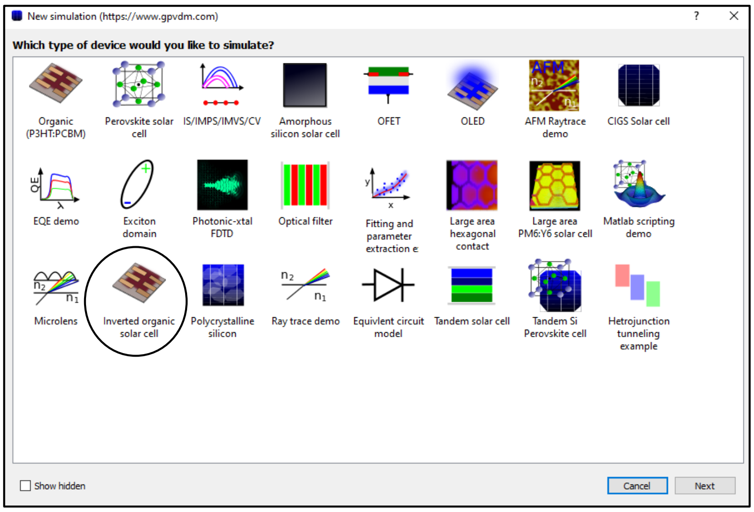

Which type of device would you like to simulate?

Figure 3.5: The IPSC structure selection

3. Select “Layer” to edit the material and thickness. To change the material, click database and select the desired material.

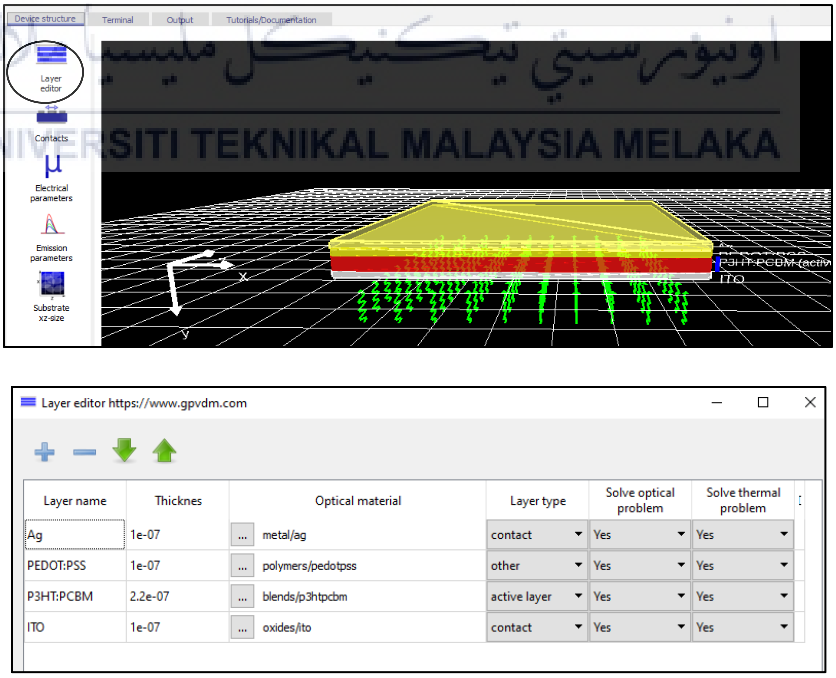

Layer name	Thicknes	Optical material	Layer type	Solve optical problem	Solve thermal problem
Ag	1e-07	metal/ag	contact	Yes	Yes
PEDOT:PSS	1e-07	polymers/pedotpss	other	Yes	Yes
P3HT:PCBM	2.2e-07	blends/p3htpcbm	active layer	Yes	Yes
ITO	1e-07	oxides/ito	contact	Yes	Yes

Figure 3.6: The window to edit the thickness and material used in GPVDM software

4. Click “Electrical parameters” to change the simulation parameter for the active layer, such as the band gap, Eg.

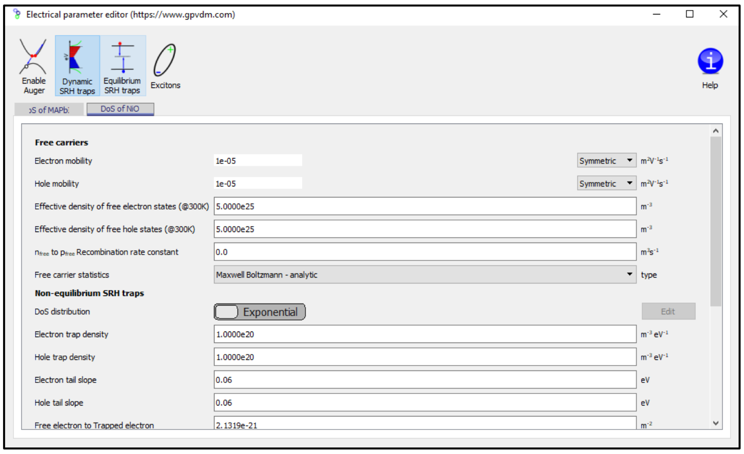

Free carriers

Electron mobility: 1e-05 Symmetric $m^2V^{-1}s^{-1}$

Hole mobility: 1e-05 Symmetric $m^2V^{-1}s^{-1}$

Effective density of free electron states (@300K): 5.0000e25 m^{-3}

Effective density of free hole states (@300K): 5.0000e25 m^{-3}

n_{free} to p_{free} Recombination rate constant: 0.0 m^3s^{-1}

Free carrier statistics: Maxwell Boltzmann - analytic type

Non-equilibrium SRH traps

DoS distribution: Exponential

Electron trap density: 1.0000e20 $m^{-3}\ eV^{-1}$

Hole trap density: 1.0000e20 $m^{-3}\ eV^{-1}$

Electron tail slope: 0.06 eV

Hole tail slope: 0.06 eV

Free electron to Trapped electron: 2.1319e-21 m^{-2}

Figure 3.7: The default value for the electrical properties of the active layer

5. Run the simulation, then click the “sim_info.dat” to know the result of important parameters such as PCE. Voc and Jsc.

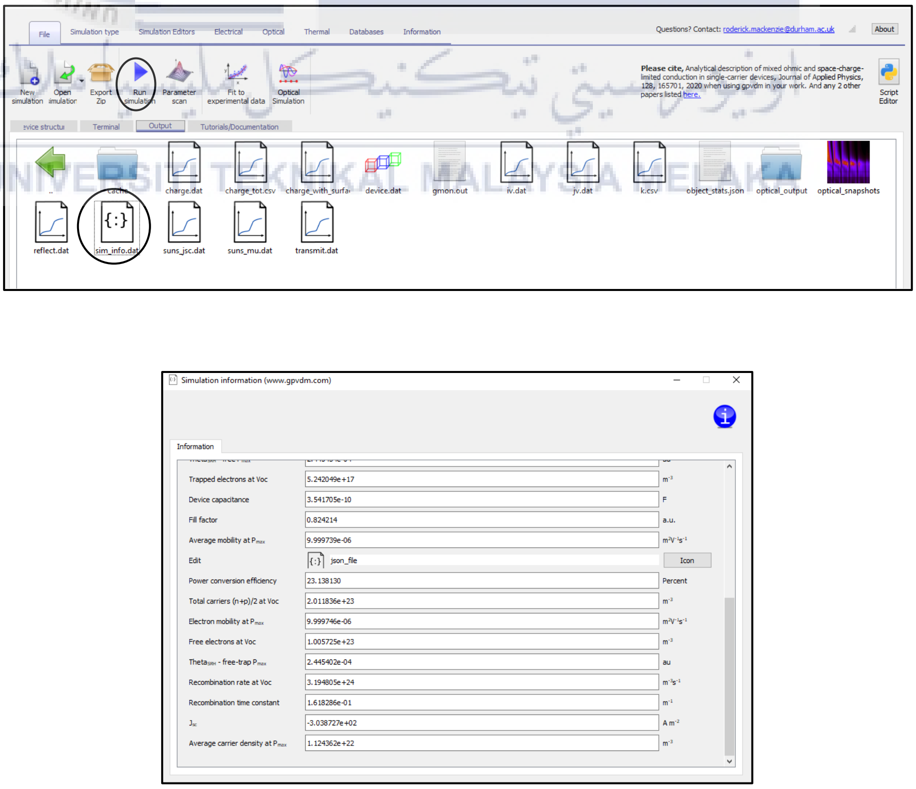

Please cite, Analytical description of mixed ohmic and space-charge-limited conduction in single-carrier devices, Journal of Applied Physics, 128, 165701, 2020 when using gpvdm in your work. And any 2 other papers listed here.

Trapped electrons at Voc: 5.242049e+17 m^{-3}

Device capacitance: 3.541705e-10 F

Fill factor: 0.824214 a.u.

Average mobility at P_{max}: 9.999739e-06 $m^2V^{-1}s^{-1}$

Edit: json_file

Power conversion efficiency: 23.138130 Percent

Total carriers (n+p)/2 at Voc: 2.011836e+23 m^{-3}

Electron mobility at P_{max}: 9.999746e-06 $m^2V^{-1}s^{-1}$

Free electrons at Voc: 1.005725e+23 m^{-3}

$Theta_{SRH}$ - free-trap P_{max}: 2.445402e-04 au

Recombination rate at Voc: 3.194805e+24 $m^{-3}s^{-1}$

Recombination time constant: 1.618286e-01 m^{-1}

J_{sc}: -3.038727e+02 $A\ m^{-2}$

Average carrier density at P_{max}: 1.124362e+22 m^{-3}

Figure 3.8: The simulation result

3.4.2 Add new material in GPVDM database

To add new material that is not previously in GPVDM database such as NiOx, the steps are:

1. Get the refractive index, α and n from previous research.

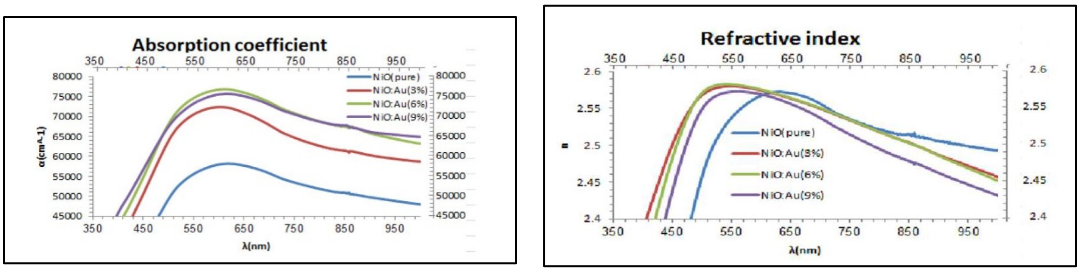

Figure 3.9: The absorbance and refractive index of NiOx [35]

2. Install a software named "Engauge Digitizer" to convert the image that containing graph, and recovers the data points from those graphs. Then, import the image and select the point by point along the desired curve.

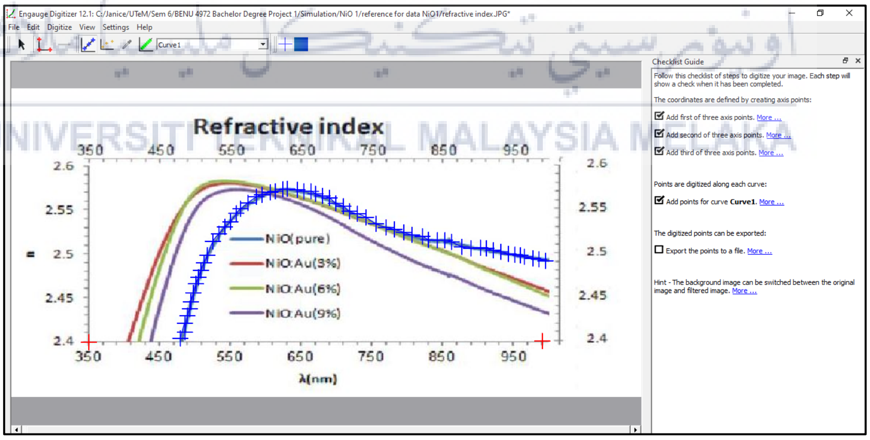
Engauge Digitizer 12.1: C:/Janice/UTeM/Sem 6/BENU 4972 Bachelor Degree Project 1/Simulation/NiO 1/reference for data NiO1/refractive index.JPG*

Checklist Guide

Follow this checklist of steps to digitize your image. Each step will show a check when it has been completed.

The coordinates are defined by creating axis points:

☑ Add first of three axis points. More ...

☑ Add second of three axis points. More ...

☑ Add third of three axis points. More ...

Points are digitized along each curve:

☑ Add points for curve **Curve1**. More ...

The digitized points can be exported:

☐ Export the points to a file. More ...

Hint - The background image can be switched between the original image and filtered image. More ...

Figure 3.10: Points along the curve

3. Extract into excel file and convert to text file. Open the GPVDM database to add the new material as shown in Figure 3.11. Then import the text file to refractive index

in the database. Make sure the y-axis and x-axis are selected properly. For the absorbance of NiOx, the step 2 and 3 are repeated. Now, the new material can be used in GPVDM as shown in Figure 3.12.

Figure 3.11: Select the “Add material” to create a new material in GPVDM database

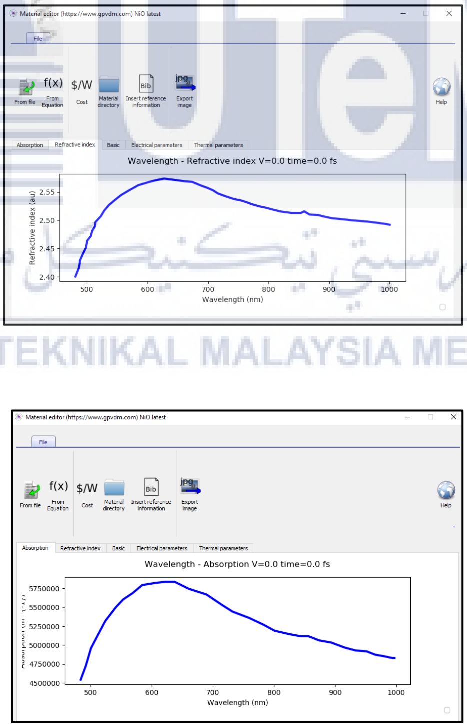

Figure 3.12: The refractive index and absorbance of NiOx is successfully added to the GPVDM

3.5 Sample Preparation

There are several deposition techniques in IPSC. Sol-gel method is selected for deposition. Students will discuss the sol-gel process for depositing NiOx/$MaPbI_3$ in this part. The steps for the experimental section are listed below.

3.5.1 Cleaning the glasses

Figure 3.13 shows the method of cleaning the glass. To begin, use a glass cutting tool to cut the glass into 2cm × 1.5cm glass (W x H). Wash the glasses with soap. Repeat this step until the glasses are washed 5 times. The glasses are then fully immersed in ethanol. Put the beaker in Ultrasonic cleaner for 30 minutes a. After 30 minutes, drain the leftover ethanol and fill the beaker with IPA. The glasses should then be sonicated for 30 minutes before being rinsed with distilled water. Remove the glasses from the beaker and place them on the petri dish. For drying the glasses, place them over the dry oven for 10 minutes.

Figure 3.13: Process of preparing clean glass

3.5.2 NiOx layer preparation

The pH meter must be calibrated before preparing the nickel oxide precursor solution. Put the pH electrode in buffer solutions of pH7, then follow by pH4 and pH10. Check that the slope efficiency is more than 92%. To make the nickel oxide precursor solution, weigh the nickel (II) acetate ($C_4H_6NiO_4$) and KOH in 0.62g and 0.56g respectively. Then prepare two solutions, which are KOH solution and $C_4H_6NiO_4$ solution.

For KOH solution, add the 0.56g KOH to 100ml distilled water. Stir the mixture at 220rpm in 30°C by using hotplate stirrer until KOH is dissolved. For $C_4H_6NiO_4$ solution, add 15ml of ethanol and 10ml of IPA with the 0.62g of nickel acetate. Stir the solution until dissolved at 210rpm in 25-26°C by using hotplate stirrer. The initial pH for this solution is pH6. Slowly add the KOH solution by using pipette to increase the pH value to pH11.

Then, raise the temperature of the hotplate stirrer to 60°C. Check the pH again after reaching 60°C. If the pH lowers, add the KOH solution again and wait 10 minutes before testing the pH. Stir the NiOx solution for 2 hours if the pH is consistently at pH11. Rest the solution for 1 day after 2 hours.

Wash with 10ml ethanol for 5 times. Each time of the washing process need to wait until there is a layer separation. Then use syringe to take out the top layer and transfer the top layer to new beaker. Refrigerate the top and bottom solutions after wrapping them with parafilm.

To begin the NiOx deposition process, sonicate the NiOx top and bottom solutions for 15 minutes. Then, drop the solution onto the glass and spin coat for 30 seconds at 3000rpm. Then, dry oven the glass for 6 minutes at 150°C before repeating the dropping and drying process 9 times more. All the process is shown in Figure 3.14.

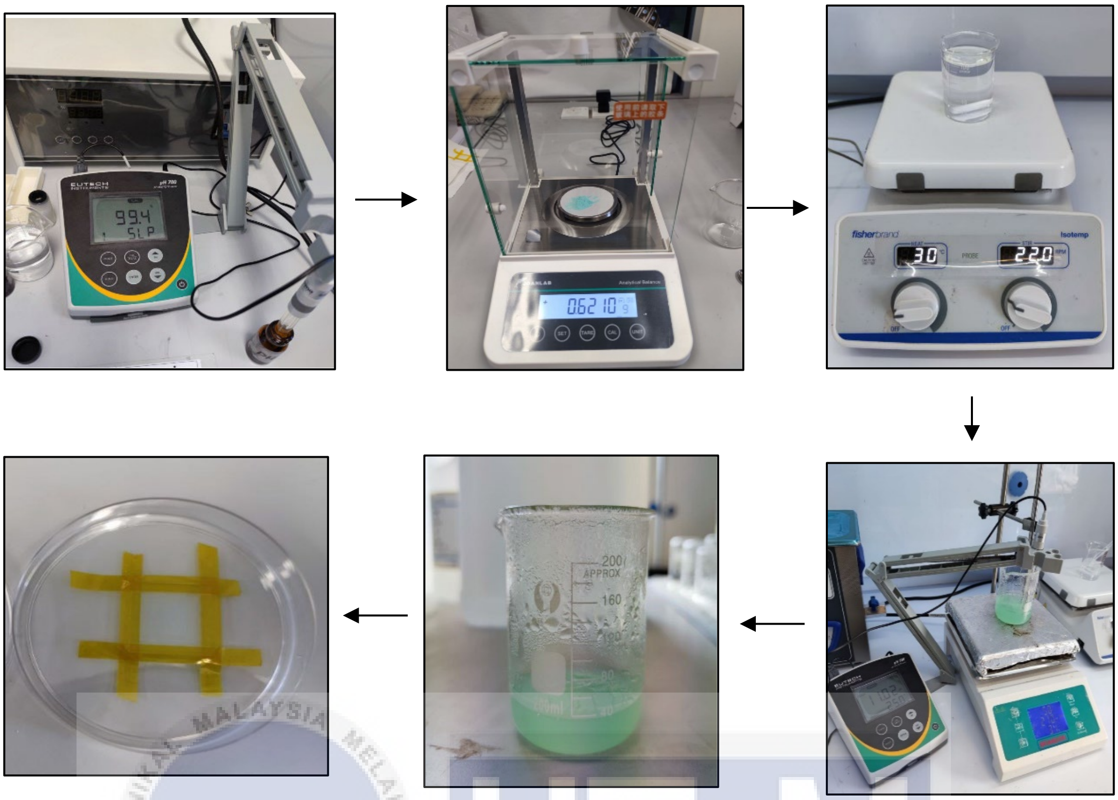

Figure 3.14: Process of preparing the NiOx layer

To anneal the NiOx film, set the temperature at 700 °C. Then the film is placed in furnace chamber as shown in Figure 3.15 when the temperature is still low. The temperature will slowly increase to the desired temperature. Leave the chamber for 1 day to collect the film to avoid the hands from being burned.

Figure 3.15: Furnace chamber

3.5.3 $MAPbI_3$ layer preparation

There are two solutions needed to be prepared in order to make the $MAPbI_3$ layer, which are MAI and PbI_2 solutions. Figure 3.16 shows the procedure for producing both solutions. To begin the preparation of the MAI solution, weigh the MAI powder with an electronic weighing machine to get 0.07g. Then, put the powder to the glass sample bottle. Fill the sample bottle with 4ml of IPA solution. The mixture is then stirred for 3 hours while maintaining a constant temperature of 20 °C and a speed of 250rpm.

Figure 3.16: Preparation of MAI and PbI_2 solutions

To prepare a PbI_2 solution, weigh 1.844g of PbI_2 on an electronic scale and place it in a new glass sample bottle. Add the 3.2ml of DMF solution gradually using the pipette. The same bottle is then filled with 0.8ml of DMSO solution. The mixture is then stirred for 3 hours at a speed of 250rpm while the temperature remains constant at 80°C. Finally, wrap the solutions in parafilm and place them in a silica box for 24 hours.

To deposit the MAI and PbI_2 solutions on glass, two step deposition method is used. Firstly, warm the NiOx film, MAI, and PbI_2 solutions for 80 °C. Using a pipette, drop the PbI_2 onto the heated glass. Check that the solution completely covers the solution. Then, spin coat for 40 seconds at 4000rpm. As seen in Figure 3.17, the glass is now yellowish in colour. Reheat the PbI_2 glass for 5 minutes on the hotplate. Drop the MAI solution on the glass, the colour of the glass should now be dark brown, as showed in Figure 3.18. Then spin coat it for 40 seconds at 4000rpm. Finally, reheat the glass for 10 minutes. The perovskite layer is now completed.

Figure 3.17: PbI_2 solution is deposited on the glass

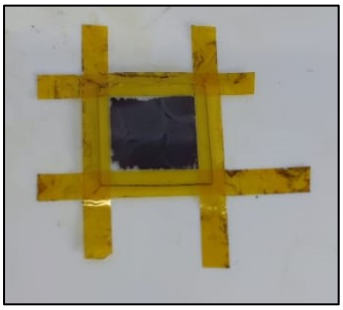

Figure 3.18: The glass after dropped with MAI solution

3.5.4 Ag layer preparation

To deposit Ag solution, use high temperature resistance tape to design the contact layer as 3x3 grid as in Figure 3.20**.** Then, heat the Ag solution at 80°C. Drop the Ag solution on the glass and lastly heat the glass at 130°C for 5 to 6 minutes.

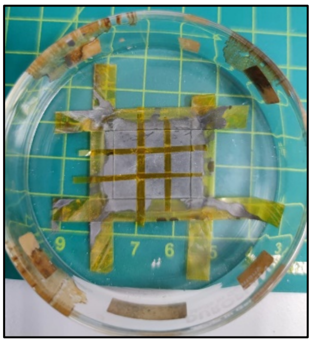

Figure 3.19: Tape the film to 3x3 grid.

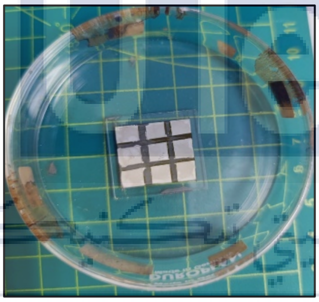

Figure 3.20: The Ag layer

CHAPTER 4

RESULTS AND DISCUSSION

This chapter basically describes about the results and also the discussion on the project that have been carried out. The results section is where the findings of the study based upon the methodology applied to gather information is reported. The results section should state the findings of the research arranged in a logical sequence without bias or interpretation. On the other hand, the purpose of the discussion section is to interpret and describe the significance of the findings in relation to what was already known about the research problem being investigated and to explain any new understanding or insights that emerged as a result the research.

4.1 Simulation by referring the reference journal

Simulate the IPSC by referring the thicknesses from the [4] which NiOx, BCP, C_{60} and perovskite are 300nm, 6.5nm, 26nm and 450nm respectively. The fabricated device in reference journal has the performance of PCE, Voc, Jsc, FF are 17.57%, 1.042V, 21.72mA cm^{-2} and 0.776 respectively. [4]

The thickness of the layers that referred from [4] is as a guidance on the thickness selection for each of the layer. There are two electrical parameters used in the simulation as shown in Table 3.1 and Table 4.1.

a) With default electrical parameter

Table 4.1: The default electrical parameter of the active layers

Parameters	NiOx	$MAPbI_3$	BCP	C60
Electron mobility ($m^2v^{-1}s^{-1}$)	1×10^{-5}	1×10^{-5}	1×10^{-5}	1×10^{-5}
Hole mobility ($m^2v^{-1}s^{-1}$)	1×10^{-5}	1×10^{-5}	1×10^{-5}	1×10^{-5}
Effective density of free electron states @300K (m^{-3})	5×10^{25}	5×10^{25}	5×10^{25}	5×10^{25}
Effective density of hole electron states (@300K) (m^{-3})	5×10^{25}	5×10^{25}	5×10^{25}	5×10^{25}
Electron affinity, Xi (eV)	1.6	1.6	1.6	1.6
Band gap, Eg (eV)	1.3	1.2	1.2	1.2
Relative permittivity	5	5	5	5

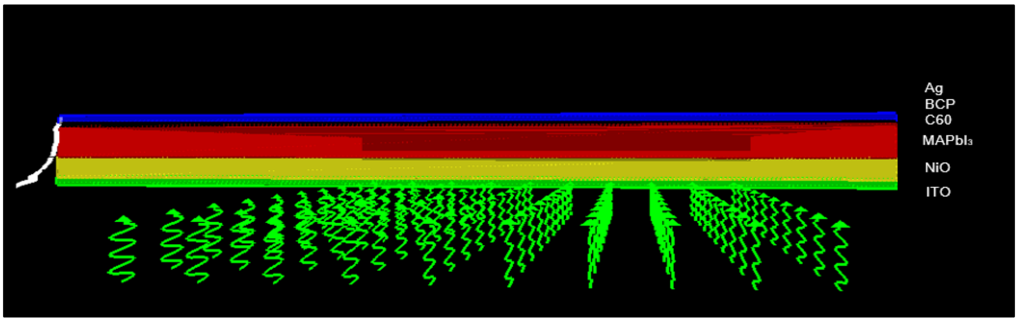

Figure 4.1: The simulated IPSC in GPVDM based on the reference thicknesses

Table 4.2: The results obtained from GPVDM when the electrical parameters are default

NiOx thickness (nm)	MAPbI3 Thickness (nm)	BCP thickness (nm)	C_{60} thickness (nm)	PCE (%)	Voc (V)	Jsc(mA cm^{-2})	FF
300	450	6.5	26	22.872	0.924	29.9	0.827

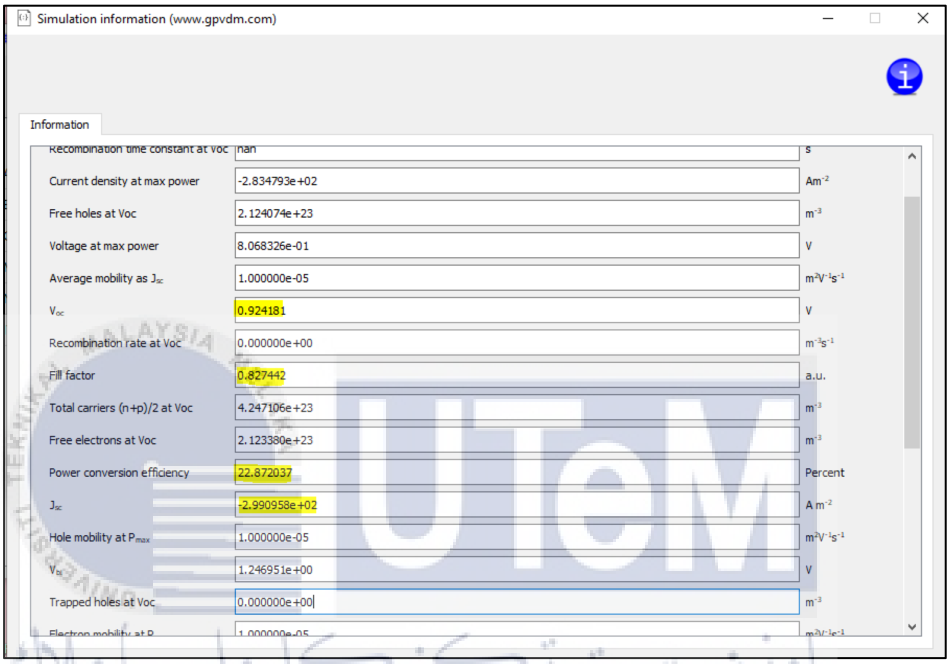

Recombination time constant at Voc	nan	s
Current density at max power	-2.834793e+02	Am^{-2}
Free holes at Voc	2.124074e+23	m^{-3}
Voltage at max power	8.068326e-01	V
Average mobility as J_{sc}	1.000000e-05	$m^2V^{-1}s^{-1}$
V_{oc}	0.924181	V
Recombination rate at Voc	0.000000e+00	$m^{-3}s^{-1}$
Fill factor	0.827442	a.u.
Total carriers (n+p)/2 at Voc	4.247106e+23	m^{-3}
Free electrons at Voc	2.123380e+23	m^{-3}
Power conversion efficiency	22.872037	Percent
J_{sc}	-2.990958e+02	$A\,m^{-2}$
Hole mobility at P_{max}	1.000000e-05	$m^2V^{-1}s^{-1}$
V_{bi}	1.246951e+00	V
Trapped holes at Voc	0.000000e+00	m^{-3}

Figure 4.2: The simulation information obtained from GPVDM

b) Included reference electrical parameter as shown in Table 3.1

Table 4.3: The results obtained from GPVDM by following the electrical parameters

NiOx thickness (nm)	MAPbI3 Thickness (nm)	BCP thickness (nm)	C_{60} thickness (nm)	PCE (%)	Voc (V)	Jsc(mA cm^{-2})	FF
300	450	6.5	26	17.347	0.727	29.91	0.798

Table 4.4: Comparison of result based on the thickness that referred from [4]

	Fabricated IPSC [4]	(a) With default electrical parameters	(b) With reference electrical parameter (material from database)
NiOx thickness (nm)	300	300	300
MAPbI3 Thickness (nm)	450	450	450
BCP thickness (nm)	6.5	6.5	6.5
C60 thickness (nm)	26	26	26
PCE (%)	17.57	22.87	17.35
Voc (V)	1.042	0.924	0.727
Jsc (mA cm^{-2})	21.72	29.9	29.91
FF	0.776	0.827	0.798

From the Table 4.4, the PCE in the simulation result of (a) is higher than the result from the reference journal. However, the simulation result (a) is not accurate as the default electrical parameters are not specified for the materials used in the structure. The simulation result of (b) is slightly lesser than the result from the referred journal but is more accurate as compared to the result of (a). This is because the electrical parameter used is referred and specified for each of the material. Therefore, optimize the IPSC by varying the thickness of the active layers such as NiOx, $MAPbI_3$, BCP and C_{60} is needed so that the performance is greater than the experimental result in [4].

4.2 Optimization

This step is to vary the thickness of HTL, perovskite and ETL layer to get the highest efficiency of the IPSC. Then, the variation on electrical parameters, α, and n in the simulation for layer of NiOx, C_{60} and BCP are analyzed to obtain the optimum PCE.

The simulation results are analyzed and grouped into three cases:

- In Case 1 uses the default electrical parameters and the materials' α and n in the GPVDM database. Thickness of NiOx, BCP and C_{60} is varied.
- In Case 2, the electrical parameters are referred to the previous experiments but remain the same thickness, α and n.
- In Case 3 is now remaining the referred electrical parameter but the α and n are extracted from the experiment data. The thickness is varied again to get the closer efficiency compared to fabricated IPSC device structure [4]

Case 1: With default electrical parameter (All material from GPVDM database, except NiOx layer)

The thickness of NiOx ranges from 50nm to 550nm. However, the thicknesses of BCP and C_{60} remain unchanged, at 6.5nm and 26nm, respectively, according to the reference journal. Figure 4.3a shows that when NiOx is 200nm, the PCE is the greatest, at 24.89%. At this thickness, the Voc, Jsc, and FF are 0.923V, 32.66mA cm^{-2}, and 0.826, respectively. The ideal thickness for NiOx is currently 200nm.

BCP is varied from 5nm to 50nm, whereas NiOx and C_{60} remain constant at 200nm and 26nm, respectively. Figure 4.3b shows that the highest PCE is 25.19% when the thickness of BCP is 30nm. At this thickness, the Voc, Jsc, and FF are 0.924V, 32.99mA cm^{-2}, and 0.826, respectively. The ideal thickness for BCP is now 30nm.

C_{60} is varied from 5nm to 50nm, where NiOx and BCP are constant, which are 200nm and 30nm respectively. The highest PCE shown in Figure 4.6c is 25.18% when C_{60} is 15nm. The Voc, Jsc and FF at this thickness is 0.924V, 33.02mA cm^{-2} and 0.826 respectively. The optimal thickness for C_{60} now is 15nm.

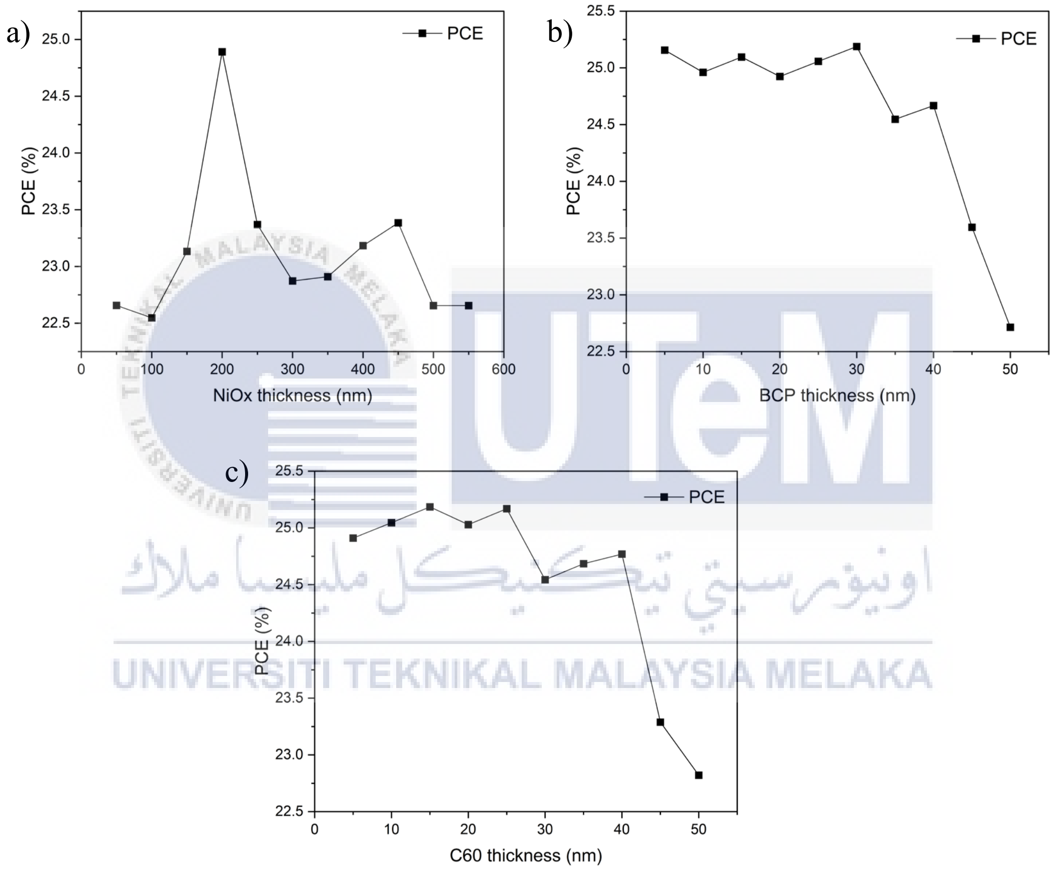

Figure 4.3: Vary the layer thickness; a) NiOx in between 50-550nm; b) Vary BCP in between 5-50nm; c) Vary C_{60} in between 5-50nm

The ideal thicknesses for NiOx, BCP, and C_{60} based on GPVDM software are now 200nm, 30nm, and 15nm, respectively, because the PCE produced is 25.18% at these thicknesses.

Case 2: Included reference electrical parameter for NiOx, MAPbI$_3$, BCP and C$_{60}$ layer. (All material from GPVDM database, except NiOx layer)

The thicknesses of active layers from Case 1 are placed in the simulation that included reference electrical parameter. Below table is result after inserting the electrical parameter in GPVDM.

Table 4.5: Result after placed the optimum thicknesses obtained from Case 1

NiOx thickness (nm)	MAPbI3 Thickness (nm)	BCP thickness (nm)	C60 thickness (nm)	PCE (%)	Voc (V)	Jsc(mA cm^{-2})	FF
200	450	30	15	18.925	0.726	33.01	0.790

The optimum thickness from Case 1 is acceptable after inserting the electrical parameters in simulation. The PCE is 18.925%, which is better than the result from [4]. However, the α and n of each material needed to insert in the software to get a more accurate result.

Case 3: Remaining the referred electrical parameter but the α and n are extracted from the experiment data.:

Table 4.6 Result after manually inserted the α and n

NiOx thickness (nm)	MAPbI$_3$ Thickness (nm)	BCP thickness (nm)	C60 thickness (nm)	PCE (%)	Voc (V)	Jsc(mA cm^{-2})	FF
200	450	30	15	13.052	0.716	22.92	0.794

The optimum thickness from Case 1 is not suitable after the materials are manually inserted the α and n for the selected layers as shown in Table 4.6. The PCE is decreased to 13.052%. Therefore, a new analysis is needed to construct again.

The thickness of NiOx ranges from 50nm to 550nm. However, the thicknesses of BCP and C_{60} remain unchanged, at 6.5nm and 26nm, respectively. Figure 4.4a showed that the PCE is greatest when NiOx is 500nm, at 17.86%. The Voc, Jsc, and FF values at this thickness are 0.733V, 30.49mA cm^{-2}, and 0.799, respectively. The optimal thickness for NiOx is presently 500nm.

BCP is changed from 5nm to 50nm, whilst NiOx and C_{60} are fixed at 500nm and 26nm, respectively. According to Figure 4.4b, the greatest PCE is 18.06% when BCP is 20nm. The Voc, Jsc, and FF values at this thickness are 0.734V, 30.83mA cm^{-2}, and 0.798, respectively. The optimal BCP thickness is now 20nm.

C_{60} is changed between 5nm and 50nm, whereas NiOx and BCP remain constant at 500nm and 20nm, respectively. The maximum PCE exhibited in Figure 4.4c is 18.227% when C_{60} is 5nm. At this thickness, the Voc, Jsc, and FF are 0.734V, 31.15mA cm^{-2}, and 0.798, respectively. The ideal thickness for C_{60} is now 5nm.

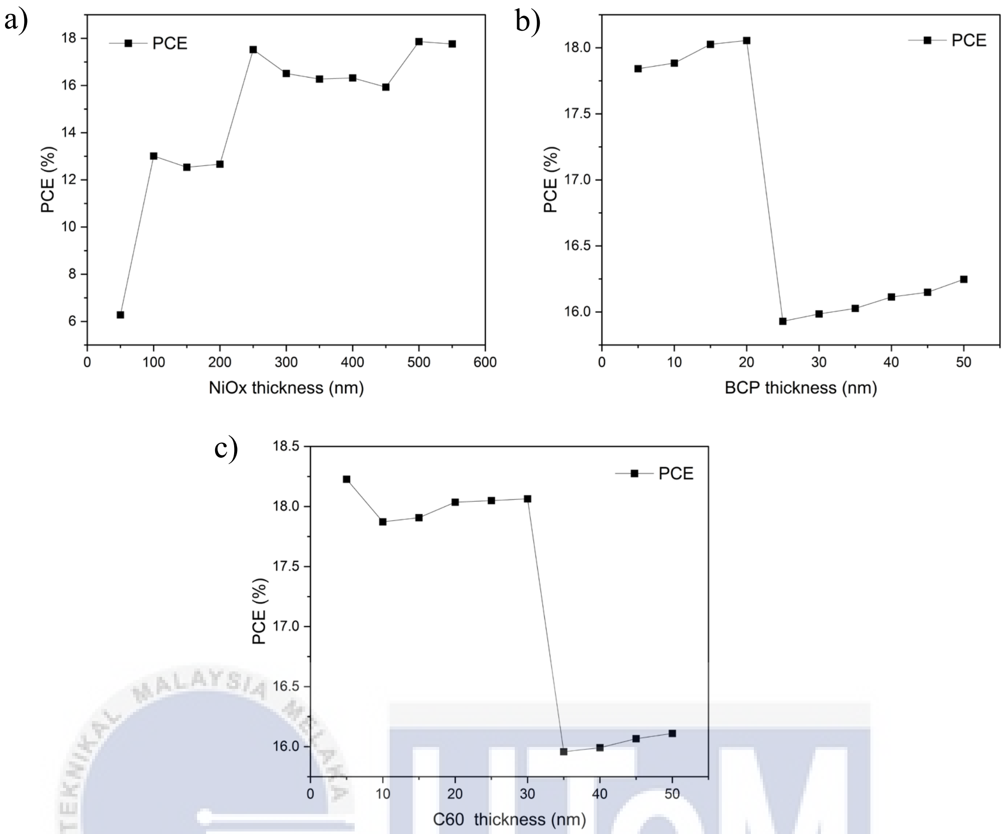

Figure 4.4: Vary layer thickness include electrical parameters and manually inserted the α and n. a) NiOx in between 50-550nm; b) BCP in between 5-50nm; c) C60 in between 5-50nm

Comparison of all the results:

Table 4.7 showed the comparison of the result of all cases. The preferable case to choose is the thickness of each layer from Case 3. The reason is that the materials' α, n and electrical parameters are taken from real experiment data from previous researches. This will cause the simulation result to be more accurate and better efficiency after the optimization as compared to reference journal. [4] Thus, the thickness of NiOx, $MAPbI_3$, BCP and C_{60} is based on the analysis for Case 3.

Table 4.7: Comparison of the result of all the cases with the result in [4]

Case	Fabricated IPSC result [4]	Simulated IPSC result (Case 1)	Simulated IPSC result (Case 2)	Simulated IPSC result (Case 3)
NiOx thickness (nm)	300	200	200	500
MAPbI3 Thickness (nm)	450	450	450	450
BCP thickness (nm)	6.5	30	30	20
C60 thickness (nm)	26	15	15	5
PCE (%)	17.57	25.185	18.925	18.227
Voc (V)	1.042	0.924	0.726	0.734
Jsc (mA cm^{-2})	21.72	32.99	33.012	31.15
FF	0.776	0.826	0.79	0.798

4.3 Simulation from GPVDM

After obtained the optimum thickness from the optimization process, below figures are the final simulation result from GPVDM.

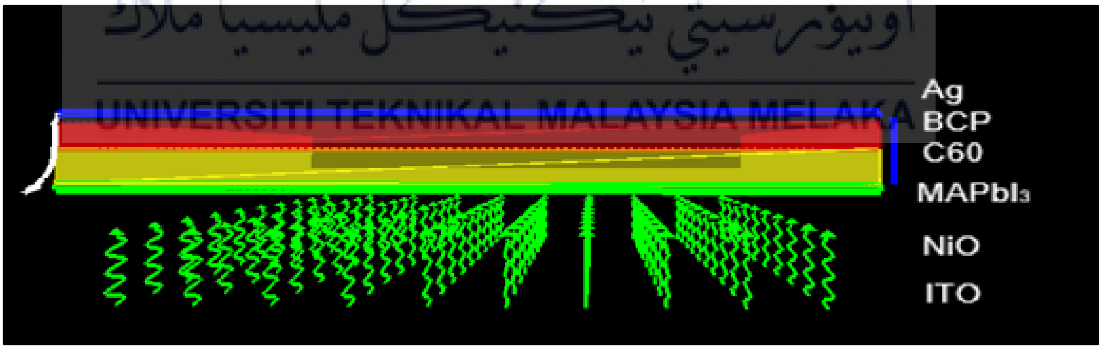

Figure 4.5: The simulated IPSC device

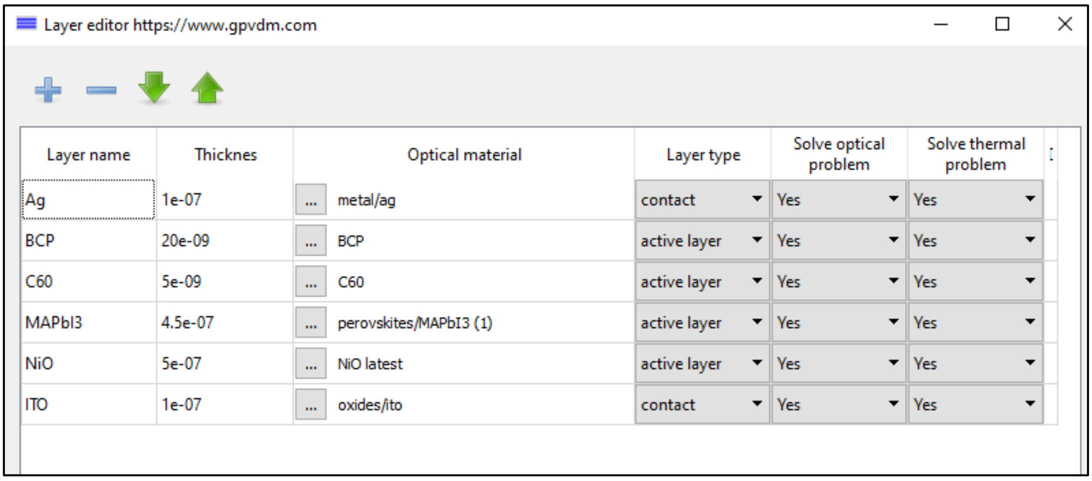

Layer name	Thicknes	Optical material	Layer type	Solve optical problem	Solve thermal problem
Ag	1e-07	metal/ag	contact	Yes	Yes
BCP	20e-09	BCP	active layer	Yes	Yes
C60	5e-09	C60	active layer	Yes	Yes
MAPbI3	4.5e-07	perovskites/MAPbI3 (1)	active layer	Yes	Yes
NiO	5e-07	NiO latest	active layer	Yes	Yes
ITO	1e-07	oxides/ito	contact	Yes	Yes

Figure 4.6: The thickness of each layer

Characteristics curve as shown in Figure 4.7 quantitatively indicate the performance of a solar cell. They show the Voc, Jsc, FF and PCE. To calculate the PCE, the formula is:

$$PCE = \frac{Jsc * Voc * FF}{100}$$

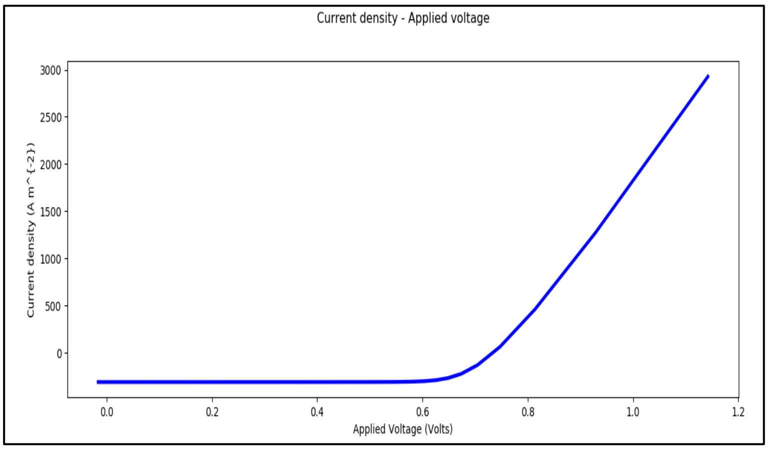

Figure 4.7: J-V characteristic curve of ITO/NiOx/MAPbI$_3$/C60/BCP/Ag

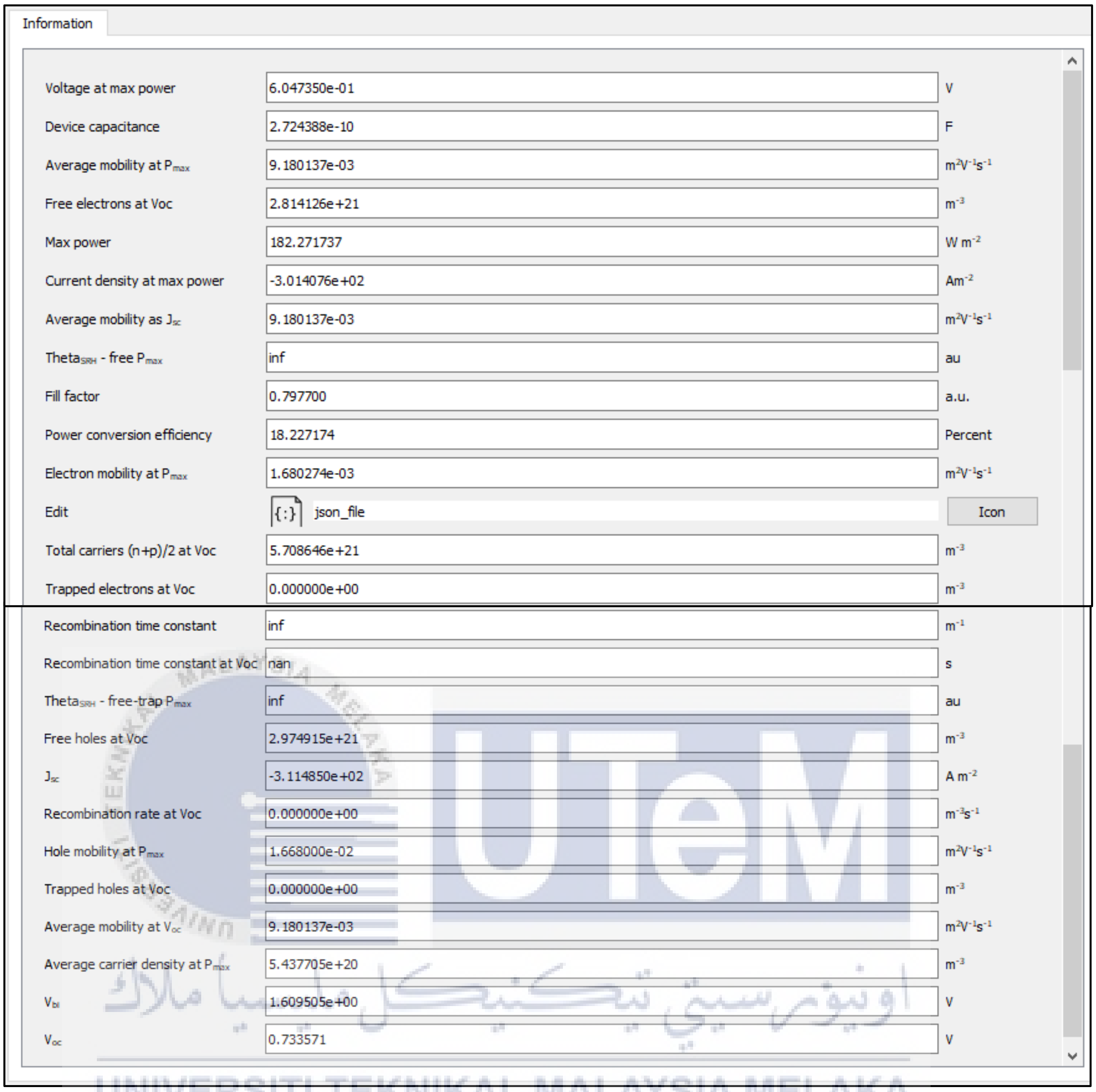

Voltage at max power	6.047350e-01	V
Device capacitance	2.724388e-10	F
Average mobility at P_{max}	9.180137e-03	$m^2V^{-1}s^{-1}$
Free electrons at Voc	2.814126e+21	m^{-3}
Max power	182.271737	W m^{-2}
Current density at max power	-3.014076e+02	Am^{-2}
Average mobility as J_{sc}	9.180137e-03	$m^2V^{-1}s^{-1}$
Theta$_{SRH}$ - free P_{max}	inf	au
Fill factor	0.797700	a.u.
Power conversion efficiency	18.227174	Percent
Electron mobility at P_{max}	1.680274e-03	$m^2V^{-1}s^{-1}$
Edit	{:} json_file	Icon
Total carriers (n+p)/2 at Voc	5.708646e+21	m^{-3}
Trapped electrons at Voc	0.000000e+00	m^{-3}
Recombination time constant	inf	m^{-1}
Recombination time constant at Voc	nan	s
Theta$_{SRH}$ - free-trap P_{max}	inf	au
Free holes at Voc	2.974915e+21	m^{-3}
J_{sc}	-3.114850e+02	A m^{-2}
Recombination rate at Voc	0.000000e+00	$m^{-3}s^{-1}$
Hole mobility at P_{max}	1.668000e-02	$m^2V^{-1}s^{-1}$
Trapped holes at Voc	0.000000e+00	m^{-3}
Average mobility at V_{oc}	9.180137e-03	$m^2V^{-1}s^{-1}$
Average carrier density at P_{max}	5.437705e+20	m^{-3}
V_{bi}	1.609505e+00	V
V_{oc}	0.733571	V

Figure 4.8: The results extracted from GPVDM

4.4 Scanning Electron Microscopes (SEM) analysis

The scanning electron microscope (SEM) is a popular tool for characterizing the morphology, topology, and detailed surface structure of solid materials. To make a fair comparison, the magnification of each film must be the same. Figure 4.9 depicts the morphology of non-anneal NiOx and annealed NiOx as determined by SEM.

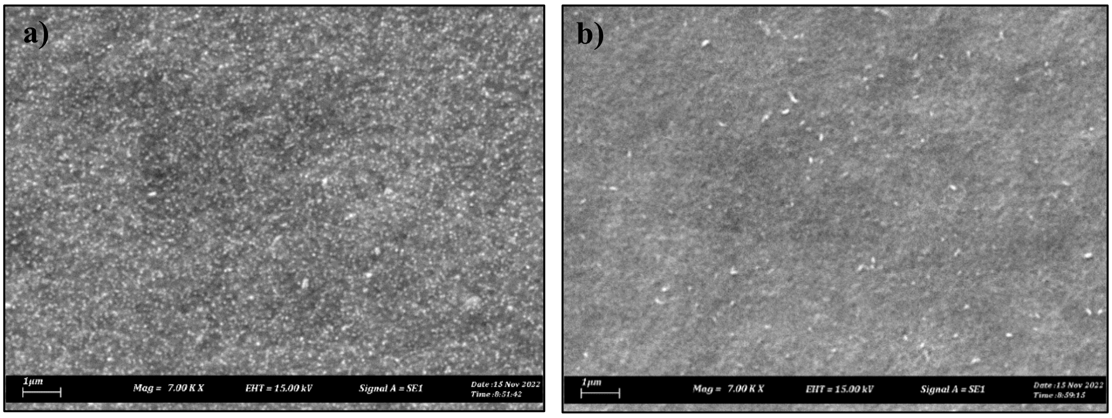

Figure 4.9: NiOx film at the magnification of 7000 a) Non-anneal NiOx b) Annealed NiOx

ImageJ software can be used to calculate the average particle size from a SEM picture. However, the minimum scale bar of the SEM picture is 1µm, and this scale still does not clearly display the NiOx particle. Hence, based on the SEM images in Figure 4.9, the particle size in Figure 4.9b is less than in Figure 4.9a.

Furthermore, by annealing the NiOx, the particle size of the NiOx is decreased. Figure 4.10 showed the SEM image of $MAPbI_3$ produced by a two-step deposition technique. The average particle size is 716.5nm, as demonstrated by the histogram in Figure 4.11.

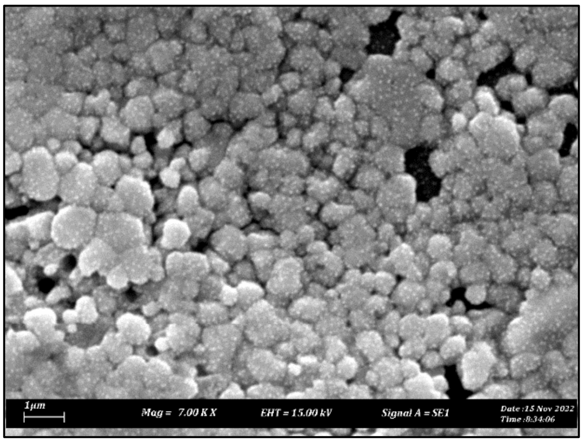

Figure 4.10: $MAPbI_3$ film at the magnification of 7000

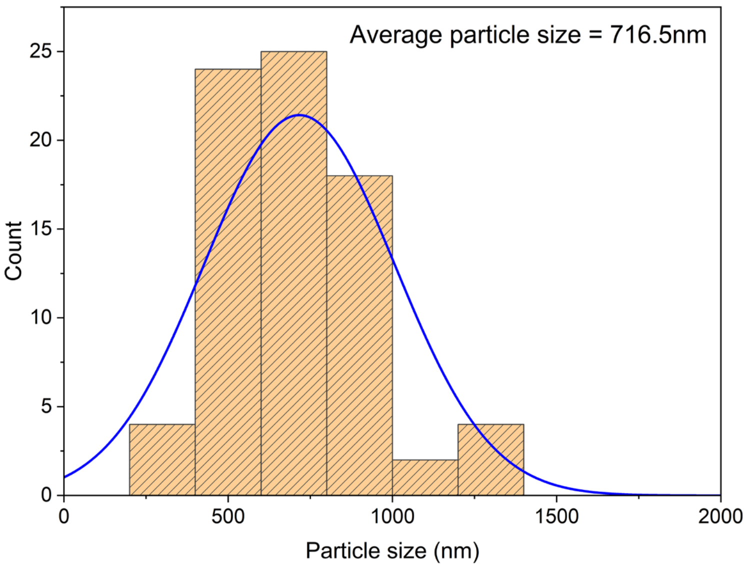

Figure 4.11: Average particle size of MAPbI$_3$

For NiOx / MAPbI$_3$ film, the observation of the SEM images in Figure 4.12 is the size particle of Figure 4.12b is smaller than the Figure 4.12a.

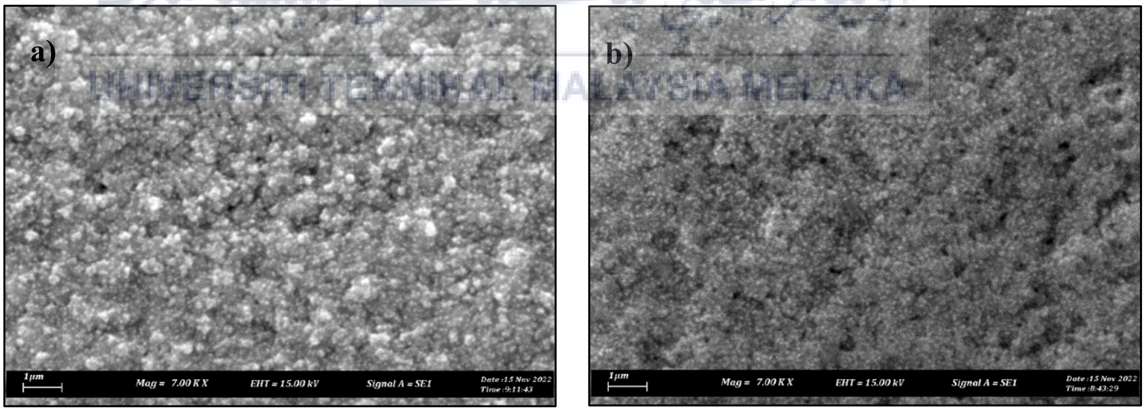

Figure 4.12: NiOx / MAPbI$_3$ film at the magnification of 7000 a) Non-anneal NiOx b) Annealed NiOx

4.5 X-ray diffraction (XRD)

X-ray diffraction (XRD) is a common method for determining the crystallinity and structure of solid materials. Figure 4.13 shows the XRD patterns of $MAPbI_3$ prepared on glass by using two step deposition method. Strong diffraction peaks are found at 14.01°, 24.53°, 28.24°, 31.95°, and 40.33° for 2θ scans, corresponding to the planes of perovskite (110), (202), (220), (310), and (224), which are consistent with prior observations of calculated XRD data for tetragonal phase of perovskite.[36]

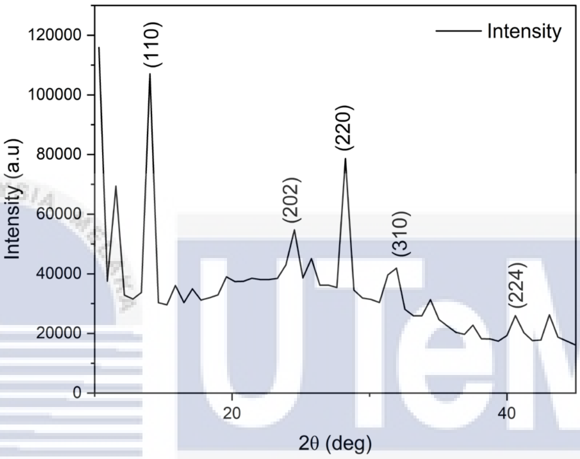

Figure 4.13: XRD pattern of $MAPbI_3$ film

However, the obtained XRD pattern for NiOx could not find the strong diffraction peak as shown in Figure 4.14. The reason is the NiOx sample is an amorphous solid, it does not give well-resolved XRD pattern.

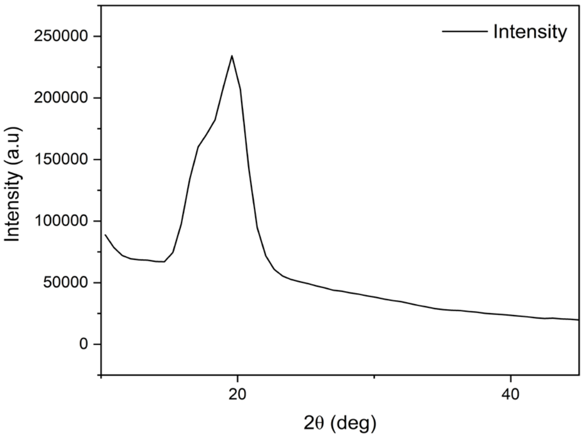

Figure 4.14: XRD pattern of NiOx film

4.6 Ultraviolet and Visible Absorption Spectroscopy (UV-Vis)

4.6.1 Absorbance of annealed NiOx and non-anneal NiOx

UV-Vis spectroscopy is used to determine the absorption spectrum of a sample. The absorption spectrum was measured by absorbance (a.u) and wavelength (nm). The range of frequency that has been selected to measure the absorption is 190nm to 1100nm.

Figure 4.15 shows the comparison of the absorbance of annealed NiOx at 700 °C and non-anneal NiOx. From this graph, the annealed NiOx film displayed the higher absorption, which is 4 a.u, towards the shorter wavelength region compared to the non-anneal NiOx film, which is 0.65 a.u at wavelength of 300nm. Also, at wavelength of 400nm, the annealed NiOx is still higher than non-anneal NiOx, which are 0.13 a.u. and 0. 06a.u respectively.

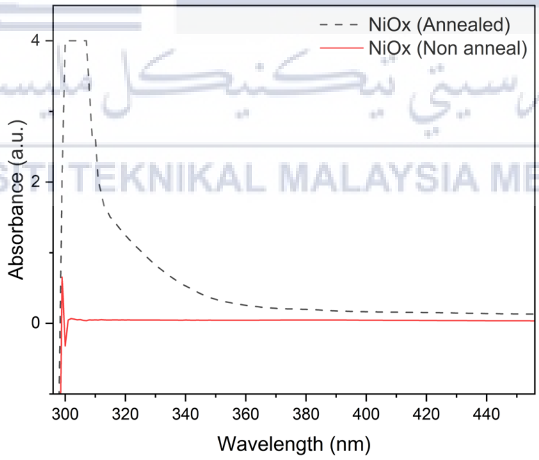

Figure 4.15: Absorbance of annealed NiOx and non-anneal NiOx

In addition, the optical bandgap can be calculated by visualising the $(\alpha hv)^2$ curve against photo energy (hv) as illustrated in Figure 4.16. Then, the Tauc plot is used for the band gap determination. This figure showed the optical band gap of the NiOx. The non-anneal NiOx has bandgap of 4.14eV while the annealed NiOx film has bandgap of 3.97eV. The annealed NiOx film is closed to the standard optical bandgap of NiOx, which is 3.84eV.[37] The reduction of energy bandgap is occurred because of the change of crystallite size.

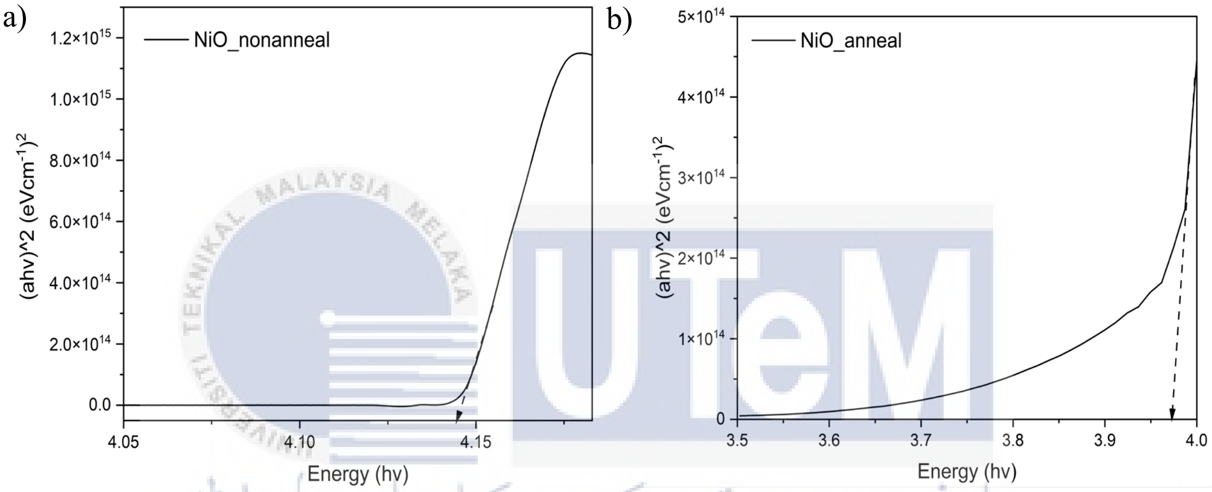

Figure 4.16: Bandgap of NiOx a) non -anneal b) annealed at 700 °C

4.6.2 Absorbance of freshly produced MAPbI3 precursor and stale $MAPbI_3$ precursor

Figure 4.17 showed the absorbance of the freshly produced $MAPbI_3$ precursor which deposited on glass and stale $MAPbI_3$ precursor that deposited on the glass. Both precursors are deposited by using two step deposition method as mentioned in Figure 3.16. The stale precursor is prepared and placed in silica gel box for a long period (3 months).

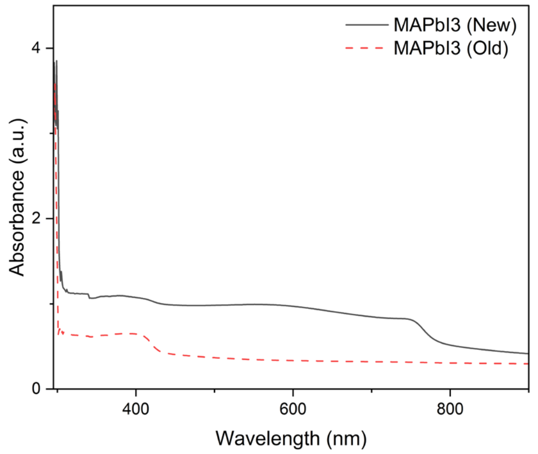

Figure 4.17: Absorbance of freshly produced MAPbI₃ precursor and stale MAPbI₃ precursor

The observation can be made from Figure 4.17 is that the absorbance for old and new $MAPbI_3$ at 400nm are 0.56 a.u and 1.05 a.u respectively. The absorbance of stale $MAPbI_3$ is lower than the newly produced $MAPbI_3$. Therefore, the degradation of $MAPbI_3$ precursor can affect the absorbance of the perovskite.

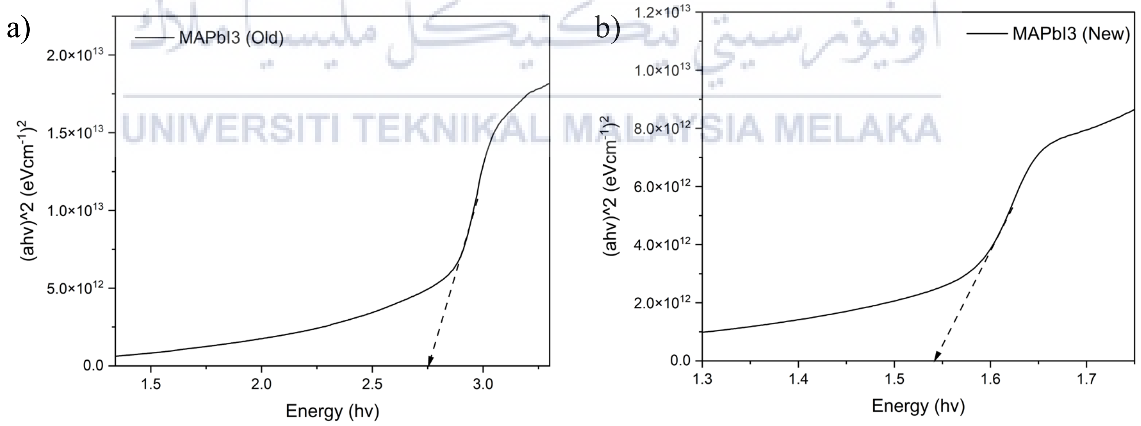

Figure 4.18: Bandgap of MAPbI₃ a) stale MAPbI₃ precursor b) freshly produced MAPbI₃ precursor

Based on Figure 4.18, the stale $MAPbI_3$ has optical bandgap of 2.75 eV, while the bandgap of fresh $MAPbI_3$ is 1.54eV. The obtained bandgap of fresh perovskite is closer to the standard optical bandgap of $MAPbI_3$, which is between 1.5 and 1.6 eV. [38]

4.6.3 Absorbance of NiOx / $MAPbI_3$

The $MAPbI_3$ is deposited on annealed NiOx film and non-anneal NiOx respectively. From the Figure 4.19, the absorbance of NiOx (annealed) / $MAPbI_3$ is higher than the absorbance of NiOx (annealed) / $MAPbI_3$, which are 1.56 a.u and 0.82 a.u. respectively at wavelength of 400nm.

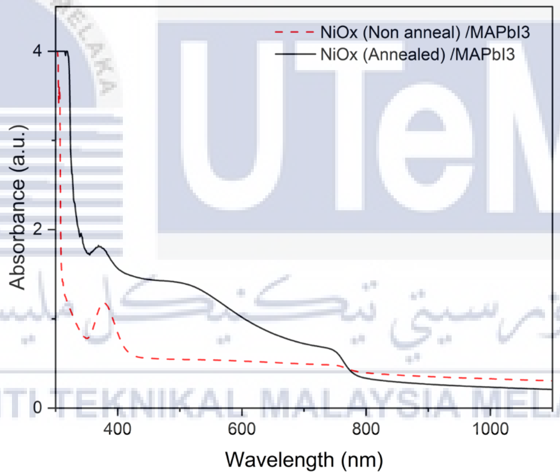

Figure 4.19: Absorbance of NiOx (annealed) / $MAPbI_3$ and NiOx (non-anneal) / $MAPbI_3$

4.7 Deposition of NiOx / $MAPbI_3$ (Degradation)

The $MAPbI_3$ was newly deposited on both of the NiOx film as shown in Figure 4.20. Based on the deposition result as shown in the figure, sample a) is darker than the sample b). The cause for the early degradation in sample b) might due to interface defects between the perovskite layer and the NiOx layer. By annealing the NiOx layer at 700 °C and then depositing perovskite on the NiOx surface, the extraction and transport of carriers at the NiOx/$MAPbI_3$ interface was expected to be increased. This is in good agreement with [39].

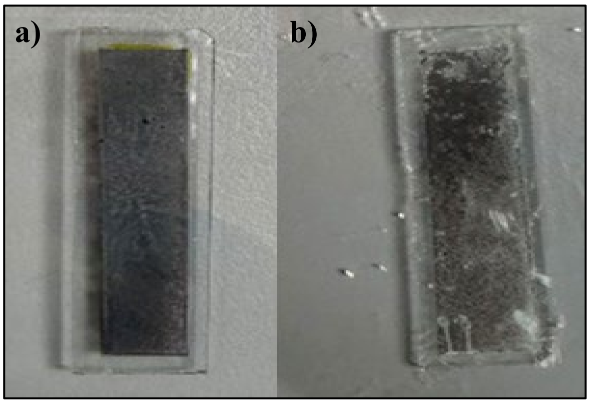

Figure 4.20: The deposited NiOx/$MAPbI_3$ layer a) annealed NiOx b) non-anneal NiOx

After 30 days, the observation can be made is that the sample b) showed that the $MAPbI_3$ is almost degraded as compared to sample a). This is shown in Figure 4.21. Therefore, with annealed NiOx, a longer shelf lifetime confirmed the stability of the device than the non-anneal NiOx.

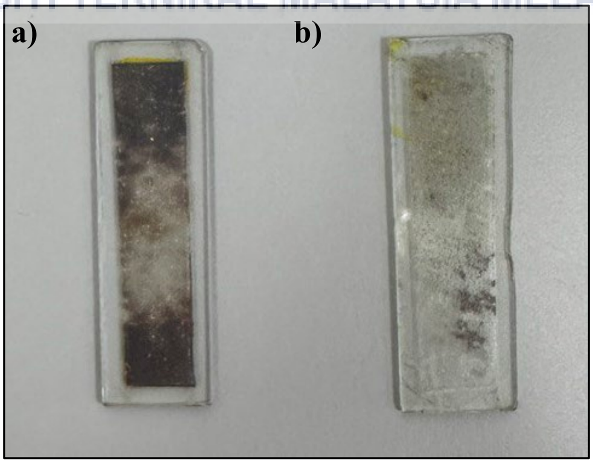

Figure 4.21: The deposited NiOx/$MAPbI_3$ after 30 days. a) annealed NiOx b) non-anneal NiOx

CHAPTER 5

CONCLUSION AND FUTURE WORKS

In this chapter, two sections are discussed. The first section reviewed and concluded this project. The second section provides suggestions on future enhancements for this project.

5.1 Conclusion

In conclusion, the first objective of this project is to simulate NiOx as HTL in the IPSC using GPVDM software is achieved. A complete modelling device structure of ITO/NiOx/$MAPbI_3$/C60/BCP/Ag is successfully simulated in GPVDM software. The thickness of NiOx, $MAPbI_3$, C_{60}, BCP and Ag are 500nm, 450nm, 5nm, 20nm and 100nm respectively.

Next, the second objective of this project is to evaluate the performance of simulated IPSC by extracting the important parameters such as PCE, FF, Voc and Jsc on different variation of layers in GPVDM software is achieved. The result from GPVDM is matched and good agreement to the fabricated IPSC device structure in previous experiment, which is 17.34% and17.57%. [4]

The simulation for Case 3 has been improved after replacing the α and n because all the parameters are from real experiment data. The result is then optimized by varying the thickness, which the PCE is 18.227%. Overall, Case 3 is the preferred case for selecting the thickness of each active layer. The simulation result of Case 3 produced an accurate and better result compared with the other cases, where the PCE, Voc, Jsc and FF are 18.227%, 0.734 V, 31.15mA cm^{-2} respectively. Therefore, the simulation must carefully insert the electrical parameter. α, n to get a more accurate result.

The third objective of this project is to deposit the NiOx/$MAPbI_3$ layer, which is synthesized by sol-gel method is achieved. Following that, several characterizations of the layer are performed. In comparison to non-anneal NiOx, annealed NiOx changed the particle size, absorbance, energy bandgap and thereby increased the extraction and transport of the carriers at the NiOx/$MAPbI_3$ layer. As a result, annealed NiOx has improved performance and stability, resulting in a longer shelf life. Furthermore, the degradation of the $MAPbI_3$ precursor can impact the absorbance of the perovskite.

Lastly, the investigation finding of NiOx/$MAPbI_3$ interfacial in IPSC can be beneficial to the development of IPSC with higher PCE.

5.2 Future work

For future works, the NiOx is in nanoscale which is hard to measure the average particle size based on the obtained SEM image. Therefore, TEM characterization is suggested which can allow for more detailed structural features and the determination of geometrical dimensions. Furthermore, NiOx sample is required to be annealed before performing XRD analysis so that diffraction peaks can be obtained in the XRD pattern.

Then, a complete modelling device structure of ITO/NiOx/$MAPbI_3$/C_{60}/BCP/Ag can be fabricated using the simulation findings as a guidance for device construction. Lastly, the four-point probe testing can be conducted for the fabricated IPSC device to measure the performance of the device.

REFERENCES

[1] A. B. Photovoltaic and B. Systems, “A Review of the Energy Performance and Life-Cycle,” 2018, doi: 10.3390/en11113157.

[2] S. Nair, S. B. Patel, and J. V. Gohel, “Recent trends in efficiency-stability improvement in perovskite solar cells,” *Mater. Today Energy*, vol. 17, p. 100449, 2020, doi: 10.1016/j.mtener.2020.100449.

[3] X. Yin, Y. Guo, H. Xie, W. Que, and L. B. Kong, “Nickel Oxide as Efficient Hole Transport Materials for Perovskite Solar Cells,” vol. 1900001, pp. 1–27, 2019, doi: 10.1002/solr.201900001.

[4] G. Shen, Q. Cai, H. Dong, X. Wen, X. Xu, and C. Mu, “Using Interfacial Contact Engineering to Solve Nickel Oxide/Perovskite Interface Contact Issues in Inverted Perovskite Solar Cells,” *ACS Sustain. Chem. Eng.*, vol. 9, no. 9, pp. 3580–3589, 2021, doi: 10.1021/acssuschemeng.0c09056.

[5] C. C. Boyd *et al.*, “Overcoming Redox Reactions at Perovskite-Nickel Oxide Interfaces to Boost Voltages in Perovskite Solar Cells,” *Joule*, vol. 4, no. 8, pp. 1759–1775, 2020, doi: 10.1016/j.joule.2020.06.004.

[6] L. Zhang, X. Liu, J. Li, and S. McKechnie, “Interactions between molecules and perovskites in halide perovskite solar cells,” *Sol. Energy Mater. Sol. Cells*, vol. 175, no. July 2017, pp. 1–19, 2018, doi: 10.1016/j.solmat.2017.09.038.

[7] S. Ameen *et al.*, “Perovskite Solar Cells: Influence of Hole Transporting Materials on Power Conversion Efficiency,” *ChemSusChem*, vol. 9, no. 1, pp. 10–27, 2016, doi: 10.1002/cssc.201501228.

[8] A. Ghosh, S. Safat, and M. S. Islam, “Stable and Efficient Perovskite Solar Cell with Metal Oxide Transport Layers,” *2nd Int. Conf. Electr. Comput. Commun. Eng. ECCE 2019*, no. March 2020, 2019, doi: 10.1109/ECACE.2019.8679418.

[9] S. Pitchaiya *et al.*, “A review on the classification of organic/inorganic/carbonaceous hole transporting materials for perovskite solar cell application,” *Arab. J. Chem.*, vol. 13, no. 1, pp. 2526–2557, 2020, doi: 10.1016/j.arabjc.2018.06.006.

[10] G. M. Arumugam *et al.*, “Inorganic hole transport layers in inverted perovskite solar cells: A review,” *Nano Sel.*, vol. 2, no. 6, pp. 1081–1116, 2021, doi: 10.1002/nano.202000200.

[11] R. Singh, P. K. Singh, B. Bhattacharya, and H. W. Rhee, “Review of current progress in inorganic hole-transport materials for perovskite solar cells,” *Appl. Mater. Today*, vol. 14, pp. 175–200, 2019, doi: 10.1016/j.apmt.2018.12.011.

[12] H. H. Park, “Efficient and stable perovskite solar cells based on inorganic hole transport materials,” *Nanomaterials*, vol. 12, no. 1, 2022, doi: 10.3390/nano12010112.

[13] F. Ma, Y. Zhao, J. Li, X. Zhang, H. Gu, and J. You, “Nickel oxide for inverted structure perovskite solar cells,” *J. Energy Chem.*, vol. 52, pp. 393–411, 2020, doi: 10.1016/j.jechem.2020.04.027.

[14] Z. Qiu *et al.*, “Enhanced physical properties of pulsed laser deposited NiO films via annealing and lithium doping for improving perovskite solar cell efficiency,” *J. Mater. Chem. C*, vol. 5, no. 28, pp. 7084–7094, 2017, doi: 10.1039/c7tc01224a.

[15] Y. Wei *et al.*, “Improving the efficiency and environmental stability of inverted planar perovskite solar cells via silver-doped nickel oxide hole-transporting layer,” *Appl. Surf. Sci.*, vol. 427, pp. 782–790, 2018, doi: 10.1016/j.apsusc.2017.08.184.

[16] J. Zhang *et al.*, “Obstructing interfacial reaction between NiOx and perovskite to enable efficient and stable inverted perovskite solar cells,” *Chem. Eng. J.*, vol. 426, no. June, p. 131357, 2021, doi: 10.1016/j.cej.2021.131357.

[17] B. Zhang *et al.*, “NiO/Perovskite Heterojunction Contact Engineering for Highly Efficient and Stable Perovskite Solar Cells,” *Adv. Sci.*, vol. 7, no. 11, 2020, doi: 10.1002/advs.201903044.

[18] V. Manjunath, S. Bimli, K. H. Parmar, P. M. Shirage, and R. S. Devan, “Oxidized Nickel films as highly transparent HTLs for inverted planar perovskite solar cells,” *Sol. Energy*, vol. 193, no. October, pp. 387–394, 2019, doi: 10.1016/j.solener.2019.09.070.

[19] I. J. Park *et al.*, “Highly Efficient and Uniform 1 cm2 Perovskite Solar Cells

with an Electrochemically Deposited NiOx Hole-Extraction Layer," *ChemSusChem*, vol. 10, no. 12, pp. 2660–2667, 2017, doi: 10.1002/cssc.201700612.

[20] H. Lee, Y. T. Huang, M. W. Horn, and S. P. Feng, "Engineered optical and electrical performance of rf-sputtered undoped nickel oxide thin films for inverted perovskite solar cells," *Sci. Rep.*, vol. 8, no. 1, pp. 1–10, 2018, doi: 10.1038/s41598-018-23907-0.

[21] T. Wang, D. Ding, X. Wang, R. Zeng, H. Liu, and W. Shen, "High-Performance Inverted Perovskite Solar Cells with Mesoporous NiO x Hole Transport Layer by Electrochemical Deposition," *ACS Omega*, vol. 3, no. 12, pp. 18434–18443, 2018, doi: 10.1021/acsomega.8b02612.

[22] A. K. Mahmud Hasan *et al.*, "Air-stable perovskite photovoltaic cells with low temperature deposited NiOx as an efficient hole-transporting material," *Opt. Mater. Express*, vol. 10, no. 8, p. 1801, 2020, doi: 10.1364/ome.391321.

[23] E. Aydin *et al.*, "Room-Temperature-Sputtered Nanocrystalline Nickel Oxide as Hole Transport Layer for p-i-n Perovskite Solar Cells," *ACS Appl. Energy Mater.*, vol. 1, no. 11, pp. 6227–6233, 2018, doi: 10.1021/acsaem.8b01263.

[24] Z. R. Marand *et al.*, "Structural and electrical investigation of cobalt-doped niox/perovskite interface for efficient inverted solar cells," *Nanomaterials*, vol. 10, no. 5, pp. 1–13, 2020, doi: 10.3390/nano10050872.

[25] J. Zhang *et al.*, "Solution-processed Sr-doped NiOx as hole transport layer for efficient and stable perovskite solar cells," *Sol. Energy*, vol. 174, no. August,

pp. 1133–1141, 2018, doi: 10.1016/j.solener.2018.10.004.

[26] and H.-C. H. Zhang-Wei Huang, Sheng-Hsiung Yang, Zong-Yu Wu, “Performance Comparison between the Nanoporous NiOx Layer and NiOx Thin Film for Inverted Perovskite Solar Cells with Long-Term Stability _ Enhanced Reader.pdf.” 2021.

[27] P. S. Chandrasekhar, Y. H. Seo, Y. J. Noh, and S. I. Na, “Room temperature solution-processed Fe doped NiOx as a novel hole transport layer for high efficient perovskite solar cells,” *Appl. Surf. Sci.*, vol. 481, no. March, pp. 588–596, 2019, doi: 10.1016/j.apsusc.2019.03.164.

[28] A. Ioakeimidis, I. T. Papadas, E. D. Koutsouroubi, G. S. Armatas, and S. A. Choulis, “Thermal analysis of metal-organic precursors for functional cu:Niox hole transporting layer in inverted perovskite solar cells: Role of solution combustion chemistry in cu:Niox thin films processing,” *Nanomaterials*, vol. 11, no. 11, pp. 1–16, 2021, doi: 10.3390/nano11113074.

[29] M. S. Shamna, K. S. Nithya, and K. S. Sudheer, “Simulation and optimization of CH3NH3SnI3 based inverted perovskite solar cell with NiO as Hole transport material,” *Mater. Today Proc.*, vol. 33, no. October 2021, pp. 1246–1251, 2019, doi: 10.1016/j.matpr.2020.03.488.

[30] S. Loke, “Photovoltaic Technologies Developed for Space-Based Solar Power,” 2022.

[31] A. bdelkade. Hima, “GPVDM simulation of layer thickness effect on power conversion efficiency of CH3NH3PbI3 based planar heterojunction solar cell,”

Int. J. Energ., vol. 3, no. 1, p. 37, 2018, doi: 10.47238/ijeca.v3i1.64.

[32] Y. Raoui, H. Ez-zahraouy, N. Tahiri, O. El, S. Ahmad, and S. Kazim, “Performance analysis of MAPbI 3 based perovskite solar cells employing diverse charge selective contacts : Simulation study,” *Sol. Energy*, vol. 193, no. February, pp. 948–955, 2019, doi: 10.1016/j.solener.2019.10.009.

[33] N. Touafek, C. Dridi, and R. Mahamdi, “Bathocuproine Buffer Layer Effect on the Performance of Inverted Perovskite Solar Cells,” pp. 1–6, 2020.

[34] X. B. 1 Yongjin Gan 1, P. M. 4, and Q. J. 3 and , Yucheng Liu 2,* , Binyi Qin 1, Qingliu Li 1, “Using Cell Capacitance Simulator,” *Numer. Investig. Energy Convers. Perform. Tin-Based Perovskite Sol. Cells Using Cell Capacit. Simulator*, 2020.

[35] S. Sagadevan and J. Podder, “Investigations on structural, optical, morphological and electrical properties of nickel oxide nanoparticles,” *Int. J. Nanoparticles*, vol. 8, no. 3–4, pp. 289–301, 2015, doi: 10.1504/IJNP.2015.073731.

[36] X. Guo, C. McCleese, C. Kolodziej, A. C. S. Samia, Y. Zhao, and C. Burda, “Identification and characterization of the intermediate phase in hybrid organic-inorganic MAPbI3 perovskite,” *Dalt. Trans.*, vol. 45, no. 9, pp. 3806–3813, 2016, doi: 10.1039/c5dt04420k.

[37] F. Chandoul *et al.*, “Investigation of the properties of nanostructured nickel oxide NiO thin films irradiated at different γ-doses,” *J. Mater. Sci. Mater. Electron.*, vol. 30, no. 1, pp. 348–358, 2019, doi: 10.1007/s10854-018-0299-z.

[38] A. M. A. Leguy *et al.*, “Experimental and theoretical optical properties of methylammonium lead halide perovskites,” *Nanoscale*, vol. 8, no. 12, pp. 6317–6327, 2016, doi: 10.1039/c5nr05435d.

[39] Y. R. Lin, Y. S. Liao, H. T. Hsiao, and C. P. Chen, “Two-step annealing of NiOx enhances the NiOx–perovskite interface for high-performance ambient-stable p–i–n perovskite solar cells,” *Appl. Surf. Sci.*, vol. 504, p. 144478, 2020, doi: 10.1016/j.apsusc.2019.144478.

[40] Príncipe, Joana & Duarte, Vera & Andrade, Luísa. (2022). Inverted Perovskite Solar Cells: The Emergence of a Highly Stable and Efficient Architecture. Energy Technology. 10. 10.1002/ente.202100952.

[41] Chen, W., Wu, Y., Fan, J., Djurišić, A. B., Liu, F. Z., Tam, H. W., Ng, A., Surya, C., Chan, W. K., Wang, D., He, Z.-B., Adv. Energy Mater. 2018, 8, 1703519. https://doi.org/10.1002/aenm.201703519

LIST OF PUBLICATIONS AND PAPERS PRESENTED

[1] Chee.C.Y., Z.A.F.M.Napiah, M.I.Idris, “Effect of Different Parameters Variation of Active Layers on The Performance of Inverted Perovskite Solar Cell.,” *International Conference on Nanoscience and Nanotechnology (ICNN)*, Butuan City. Philippines, 2022.